RIGA TECHNICAL UNIVERSITY

Līga Maskova

ESTIMATION AND EXTENSION OF THE CYCLE LIFE OF $LiNi_XCo_YMn_{1-X-Y}O_2$ CATHODE MATERIAL FOR Li-ION BATTERIES

Summary of the Doctoral Thesis

RTU Press
Riga 2026

RIGA TECHNICAL UNIVERSITY
Faculty of Natural Sciences and Technology
Institute of Technical Physics

Līga Maskova
Doctoral Student of the Study Programme "Chemistry, Materials Science and Engineering"

ESTIMATION AND EXTENSION OF THE CYCLE LIFE OF $LiNi_xCo_yMn_{1-x-y}O_2$ CATHODE MATERIAL FOR LI-ION BATTERIES

Summary of the Doctoral Thesis

Scientific supervisors
Dr. phys.
GINTS KUČINSKIS
Professor Dr. habil. phys.
MĀRIS KNITE

RTU Press
Riga 2026

Maskova, L. Estimation and Extension of the Cycle Life of $LiNi_xCo_yMn_{1-x-y}O_2$ Cathode Material for Li-Ion Batteries. Summary of the Doctoral Thesis. Riga: RTU Press, 2026. 49 p.

Published in accordance with the decision of the Promotion Council "RTU P-02" of October 13th 2025, Minutes No. 04030- 9.2/9.

The research has been carried out as part of the Latvian Council of Science project "Cycle Life Prediction of Lithium-Ion Battery Electrodes and Cells, Utilizing Current-Voltage Response Measurements", No LZP-2020/1–0425 and the M-Era.net project "Inert Coatings for Prevention of Ageing of NMC Cathode for Lithium-Ion Batteries" (InCoatBat)", No 10341.

The research has been completed with the support of a PhD grant from the project No 5.2.1.1.i.0/2/24/I/CFLA/003 "Implementation of Consolidation and Management Changes at Riga Technical University, Liepaja University, Rezekne Academy of Technology, Latvian Maritime Academy and Liepaja Maritime College for the Progress towards Excellence in Higher Education, Science and Innovation" funded by the EU Recovery and Resilience Facility.

Cover picture from www.shutterstock.com.

https://doi.org/10.7250/9789934372520
ISBN 978-9934-37-252-0 (pdf)

DOCTORAL THESIS PROPOSED TO RIGA TECHNICAL UNIVERSITY FOR THE PROMOTION TO THE SCIENTIFIC DEGREE OF DOCTOR OF SCIENCE

To be granted the scientific degree of Doctor of Science (PhD.), the present Doctoral Thesis has been submitted for the defence at the open meeting of RTU Promotion Council on January 23rd 2026 at 09.30, at the Faculty of Natural Sciences and Technology of Riga Technical University, Paula Valdena Street 3/7, Room 272.

OFFICIAL REVIEWERS

Professor Dr. habil. phys. Uldis Rogulis,
Institute of Solid State Physics, University of Latvia, Latvia

Dr. phys. Raimonds Meija,
Riga Stradins University, University of Latvia, Latvia

Associate Professor Dr. Linas Vilčiauskas,
Center for Physical Sciences and Technology (FTMC), Lithuania

DECLARATION OF ACADEMIC INTEGRITY

I hereby declare that the Doctoral Thesis submitted for the review to Riga Technical University for the promotion to the scientific degree of Doctor of Science (PhD.) is my own. I confirm that this Doctoral Thesis has not been submitted to any other university for the promotion to a scientific degree.

Līga Maskova ……. (signature)
Date: ……

The Doctoral Thesis has been written in English. It consists of an Introduction, three chapters, Conclusion, 24 figures, four tables, and one appendix. The total number of pages is 101, including appendices. The Bibliography contains 200 titles.

ACKNOWLEDGEMENTS

Above all, my appreciation extends towards both of my scientific supervisors – Gints Kucinskis and Maris Knite – who led me to become a more independent and capable researcher. Their guidance, efforts, and time is what will shape my future as a scientist. Besides my direct supervisors, I would like to thank all my colleagues, also from other laboratories, for their guidance. In addition to being extremely helpful and forthcoming, most of my colleagues have genuinely cared for me and helped me through some tough times, which gave me strength to continue – for this I wish to thank everyone, but especially Rita Leimane, Gints Kucinskis, Inara Nesterova, Paula Malnaca, and Kaspars Kaprans!

I would not have completed this mountain of a task if I had not had the support of the people in my life. Firstly, I wish to express my full gratitude to my Sirsniņa – Andris Maskovs! Thank you for the unwavering support and holding space for me to grow. Secondly, I would like to thank the rest of my family with all my heart! My sisters – Rasa, Marta, Anna, and Laura – and my brothers – Miks and Māris – I can always rely on you for good laughs! Thirdly, thank you, Dad, so much, for supporting me! And, finally, I wish to thank you, Mom! You made me the person I am today.

My gratitude also extends to my friends who have been very patient with me throughout the thesis-writing journey and are just a joy to be around! Thank you, Ībļi (Zane, Daira, and Ralfs), Dita, Alma, Haralds, Kristīne, and Dace!

Finally, I would like to acknowledge my little Peciņa. Although never here, you gave me the strength to finish this and carry on, and I will love you forever…

Thank you!

TABLE OF CONTENTS

GLOSSARY

AIP – aluminum isopropoxide, $Al(OC_3H_7)_3$
BV – Butler-Volmer
CAM – cathode active material
CC – constant current
CCCV – constant current, constant voltage
CE – Coulombic efficiency
CEI – cathode-electrolyte interphase
EDS – energy-dispersive X-ray spectroscopy
EoL – end of life
EV – electric vehicle
FEC – fluoroethylene carbonate
ICP-MS – inductively coupled plasma mass spectrometry
IRMS – isotope ratio mass spectrometry
LAM – loss of active material
LCO – $LiCoO_2$
LFP – $LiFePO_4$
LIB – Li-ion battery
LLI – loss of lithium inventory
NCM – $LiNi_xCo_yMn_{1-x-y}O_2$
NMP – N-methyl-2-pyrrolidone
OCV – open circuit voltage
PVDF – polyvinylidene fluoride
RLC – residual lithium compound
SEM – scanning electron microscopy
SoC – state of charge
SoH – state of health
STEM – scanning transmission electron microscopy
TEM – transmission electron microscopy
TM – transition metal
XPS – X-ray photoelectron spectroscopy
XRD – X-ray diffraction

GENERAL DESCRIPTION OF THE RESEARCH

Introduction

Lithium-ion batteries (LIBs) have become indispensable in modern energy storage applications, powering everything from consumer electronics to electric vehicles. Their widespread application generates large amounts of waste, the recycling of which requires plenty of energy and human resources. Understanding and limiting the rate of ageing of LIBs and their components, mainly the cathode material, would thus decrease the amount of battery waste generated.

A key insight into LIB ageing pertains to the evolution of voltage hysteresis during battery cycling. As the cell degrades or is subjected to higher currents, the hysteresis in the charge-discharge curve widens. Within the scope of the Doctoral Thesis a correlation between state-of-health (SoH) and voltage hysteresis has been established for state-of-the-art $LiNi_{0.8}Co_{0.1}Mn_{0.1}O_2$ (NCM811) LIBs, allowing SoH estimation via two methods: a direct function of hysteresis, which is linear above 70 % SoH and exponential below, and through a fitting of C rate measurements with a Butler–Volmer-like function. These tools offer non-invasive methods for diagnosing battery health.

Among the various cathode chemistries employed, nickel-rich layered oxide materials, particularly $LiNi_xCo_yMn_{1-x-y}O_2$ (NCMs), have emerged as promising candidates due to their high energy density and relatively low cost. However, the increased nickel content that enhances capacity also introduces critical challenges related to material degradation, especially during prolonged cycling and high-voltage operation [1]. Understanding and mitigating the degradation mechanisms of NCM cathodes, especially those with high nickel content, is therefore essential for extending battery life and ensuring reliable performance.

Ageing in NCM cathode materials manifests through both surface and bulk degradation, with bulk degradation becoming increasingly prominent at higher states of charge (SoC), particularly beyond 80 % [2]. For high-Ni content NCMs ($\geq$ 80 %), such SoC levels are reached at lower voltages (~4.3 V) compared to lower-Ni variants (~4.6 V), making them more susceptible to structural degradation such as microcracking. This highlights a fundamental limitation in the structural resilience of high-Ni materials, requiring strategies that go beyond surface stabilisation alone, such as doping or structural modification.

To address these challenges, numerous strategies, including surface coating and elemental doping, have been explored. A meta-analysis of ageing mitigation strategies (coating and doping) conducted within the Doctoral Thesis reveals a composition-dependent trend: while surface protection plays a dominant role in NCM111, doping becomes increasingly critical for NCM622 and reaches equal importance with surface protection in NCM811. These findings underscore the necessity of combining surface protection and doping to effectively stabilise high-Ni NCMs where bulk-related degradation dominates.

Additionally, the efficacy of surface coatings is influenced not just by the coating material, but also by the processing methods. Wet-chemical procedures, commonly used for applying coatings, can inadvertently introduce degradation through solvent interactions, such as ethanol washing leading to carbonate impurity formation as demonstrated in the present Doctoral Thesis. However, subsequent sintering has been shown to reverse much of this degradation both in literature [3] and in the Doctoral Thesis. This emphasises the importance of carefully designed reference samples when evaluating coating effectiveness, as misattributing improvements to the coating effect alone can lead to misleading conclusions.

In this context, a wet-chemically applied $Al_2O_3/LiAlO_2$ coating developed within the Doctoral Thesis has shown promising results compared to a properly prepared reference sample. For NCM111, this coating method improved capacity retention from 65 % in the pristine samples to 79 % in the reference samples, to 88 % in the coated samples after 500 cycles at 1 C. Similarly, the capacity retention of NCM811 improved from 44 % in the re-sintered reference material to 54 % in the coated samples. While the absolute improvement is less pronounced in NCM811, due to the dominance of microcracking, which coatings cannot fully prevent, the relative gain still represents a meaningful advancement in extending battery lifespan.

Aim of the Doctoral Thesis

The Doctoral Thesis aims to explore the possibility of applying a simple voltage hysteresis measurement for the determination of the SoH of a LIB, as well as prolong the cycle life of NCM cathodes with the use of a protective coating, simultaneously establishing a proper reference for comparison.

Tasks

To establish a relationship between SoH and voltage hysteresis and determine the best-fit function to describe this relationship. To evaluate the possibility of determining the SoH from a simple voltage hysteresis measurement. To consider alternatives.

To conduct a meta-analysis on the coating and doping effect on capacity retention and determine the dominant ageing mechanisms in NCM cathode materials based on Ni content.

To develop a sustainable wet-chemical method to coat NCM cathodes with an inert protective coating. To establish a proper reference for the coating study. To achieve cycle life extension for the coated sample when compared to the proper reference.

Scientific Novelty

Based on available information, there is no simple method to determine the SoH of a given battery of unknown history, as the SoH of a battery is usually based on its initial state. Thus, knowing the SoH at any point would require storing large amounts of data or knowing where the battery came from. The Doctoral Thesis explores the possibility of using a simple voltage hysteresis

measurement to determine the SoH with a certain precision. This could greatly simplify the assessment of used batteries for possible second life applications.

Currently, high-nickel NCMs (Ni ≥ 80 %), despite their advantageous capacity (> 200 mAh/g), are not dominating the market due to their intrinsic stability issues. Coating the active material has been shown to improve stability; however, it is typically achieved using slow and costly methods (ALD) or toxic substances such as toluene or trimethyl aluminium. The second part of the Doctoral Thesis focuses on improving the stability of the state-of-the-art NCM cathode materials by developing a coating method that omits often-used harmful chemicals and is possible to up-scale, thus prolonging the lifetime of NCM batteries sustainably.

Practical Significance

A simple method for the determination of the SoH of batteries from scrap yards could enable assessment of their possible use in second-life applications, thus reducing the amount of dangerous waste that needs to be recycled.

When considering the currently used cathode materials with the highest energy densities, most of them contain cobalt or suffer from stability issues. The proposed wet-chemical coating method is sustainable and can be transferred to industrial scale to enable low-Co, high energy density cathode materials to enter the market.

Approbation of the Research

The results of the research conducted within the Doctoral Thesis have been published in three journal articles, all indexed in SCOPUS and Web of Science. The results have been presented at nine international scientific conferences.

Research projects and programmes

1. Latvian Council of Science project "Cycle Life Prediction of Lithium-Ion Battery Electrodes and Cells, Utilizing Current-Voltage Response Measurements", No LZP-2020/1–0425.
2. M-Era.net project "Inert Coatings for Prevention of Ageing of NMC Cathode for Lithium-Ion Batteries" (InCoatBat), No 10341.
3. Grant from the project No 5.2.1.1.i.0/2/24/I/CFLA/003 "Implementation of Consolidation and Management Changes at Riga Technical University, Liepaja University, Rezekne Academy of Technology, Latvian Maritime Academy and Liepaja Maritime College for the Progress towards Excellence in Higher Education, Science and Innovation" funded by the EU Recovery and Resilience Facility.

Publications

1. **Maskova**, **L**., Ignatans, R., Viksna, A. Sarakovskis, A., Knite, M., Kucinskis, G. (2024). Wet-Chemical Synthesis of a Protective Coating on NCM111 Cathode: The Quantified Effects of Washing, Sintering and Coating. *J. Electrochem. Soc., 171*, 100520. https://doi.org/10.1149/1945-7111/ad8483.
    - The author's contribution: L. Maskova was responsible for conceptualisation, including the development of synthesis procedure and measurement methodology, all data curation, electrochemical measurement, SEM image and XRD data acquisition and analysis, visualisation and writing the original draft, producing images except for TEM result image, reviewing and editing together with the co-authors to produce the finalised version of the paper.
2. Hodakovska, J., **Britala (Maskova)**, **L**., Mezulis, A., Grinberga, L., Bajars, G., Kucinskis, G. (2024). State of Health as a Function of Voltage Hysteresis in Li-Ion Battery Half-Cells. *Journal of Solid State Electrochemistry, 29*, 4187–4198. https://doi.org/10.1007/s10008-024-05944-0.
    - The author's contribution: J. Hodakovska and L. Britala (Maskova) contributed equally. L. Britala (Maskova) was responsible for conceptualisation, all data curation and analysis, methodology, visualisation, producing all images, writing the original draft, review and editing of the part concerning NCM 811 cathode material.
3. **Britala (Maskova)**, **L**., Marinaro, M., Kucinskis, G. (2023). A Review of the Degradation Mechanisms of NCM Cathodes and Corresponding Mitigation Strategies. *Journal of Energy Storage, 73*, 108875. https://doi.org/10.1016/j.est.2023.108875.
    - The author's contribution: L. Britala (Maskova) was responsible for conceptualisation, including defining the subject of review, all data curation for the meta-analysis, conducting the meta-analysis, visualisation and writing the original draft, producing all images, reviewing and editing together with the co-authors to produce the finalised version of the paper.

Participation in conferences

1. Britala, L., Knite, M., Kucinskis, G. (2024). Wet-Chemical Al_2O_3 Coating Synthesis for Cycle Life Extension of NCM Cathodes in Li-Ion Batteries. In: *Battery 2030+ Annual Conference 2024, Book of Abstracts*, 28–29 May 2024, Grenoble, France. Poster presentation.
2. Britala, L., Knite, M., Kucinskis, G. (2024). Development of a Wet-Chemical Al_2O_3 Coating Synthesis on $LiNi_{0.33}Co_{0.33}Mn_{0.33}O_2$ (NCM111) Electrode Material for Cycle Life Extension of Li-Ion Batteries. In: *8th Baltic Electrochemistry Conference: Finding New Inspiration 2, 2024 Book of Abstracts*, 14–17 April 2024, Tartu, Estonia. Oral presentation.

3. Britala, L., Knite, M., Kucinskis, G. (2024). Ageing Prevention of Li-Ion Batteries by Al_2O_3 Coating. In: *40th Scientific Conference of ISSP UL 2024, Book of Abstracts*, 5–7 March 2024, Riga, Latvia. Oral presentation.
4. Britala, L., Knite, M. & Kucinskis, G. (2023). A Facile Synthesis of Al_2O_3-Coated $LiNi_{1/3}Co_{1/3}Mn_{1/3}O_2$ with Improved Cycle Life Prepared by a Wet-Chemical Method. In: *ECS Meeting Abstracts MA2023-02, 3049*, 8–12 October 2023, Gothenburg, Sweden. Poster presentation.
5. Britala, L., Knite, M., Kucinskis, G. (2023). Fast Determination of the Stage of Ageing of Lithium-Ion Batteries Based on Simple Electrochemical Measurements. In: *39th Scientific Conference of ISSP UL 2023, Book of Abstracts*, 28 February–2 March 2023, Riga, Latvia. Oral presentation.
6. Britala, L., Knite, M., Kucinskis, G. Inert Coatings for Cycle Life Extension of Cathodes for Li-Ion Batteries. In: *73rd Annual Meeting of the International Society of Electrochemistry, Book of Abstracts*, 23–28 October 2022, Xiamen, Fujian, China (online). Poster presentation.
7. Britala, L., Knite, M., Kucinskis, G. (2022). Inert Coatings for Cycle Life Extension of Cathodes for Li-Ion Batteries. In: *Materials Science and Applied Chemistry 2022, Book of Abstracts*, 21 October 2022, Riga, Latvia. Oral presentation.
8. Britala, L., Knite, M., Kucinskis, G. (2022). Inert Coatings for Cycle Life Extension of Cathodes for Li-Ion Batteries. In: *FM&NT – NIBS 2022, Book of Abstracts* (p. 239), 4–6 July 2022, Riga, Latvia, online. Poster presentation.
9. Britala, L., Knite, M., Kucinskis, G. (2022). Inert Coatings for Cycle Life Extension of Cathodes for Li-Ion Batteries. In: *38th Scientific Conference of ISSP UL 2022, Book of Abstracts*, 22–24 February 2022, Riga, Latvia. Oral presentation.

THESIS STATEMENTS TO BE DEFENDED

1. Voltage hysteresis increases as the state of health (SoH) of NCM811-lithium half-cells decreases, allowing SoH assessment based on this correlation using a quick and simple voltage hysteresis measurement.
2. Improvement in capacity retention from coating or doping NCM cathode materials with different Ni content indirectly indicates the dominant (surface or bulk) aging mechanisms in these materials – larger improvements from surface coating indicate dominant surface aging mechanisms (formation of a cathode-electrolyte interphase, dissolution of transition metals, surface phase transitions, and oxygen evolution), while larger improvements from doping indicate dominant bulk aging mechanisms (cation mixing, microcrack formation).
3. The chemical coating process, involving mixing the material to be coated in a solvent and heating it at high temperatures, changes the surface structure and composition of the material, which, if left unaccounted for, leads to ambiguous conclusions about how the effect of the coating itself changes cycling stability.
4. A simple, sustainable, ethanol-based wet-chemical coating synthesis on NCM cathode materials with different Ni compositions improves their long-term cycling stability in Li-ion cells by hindering degradation of the cathode material surface.

MAIN RESULTS OF THE THESIS

Literature Review

Li-ion batteries (LIBs), the most popular kind of rechargeable batteries, have been studied for decades. Although lithium shows good performance and light weight, due to its high reactivity and fire hazard, it was only first commercialized by Sony in 1991, when the risks were somewhat neutralized by careful engineering. Coinciding with the wireless revolution, the emergence of rechargeable batteries in the 1990s paved a way for more convenient and sustainable mobile phones.

A typical LIB consists of a cathode, anode, separator, electrolyte, current collectors, all enveloped in a battery cell casing. The most important components of LIBs, which ensure that energy can be stored and obtained, are cathode and anode materials. The operating voltage and capacity of a battery cell is mainly limited by the cathode properties, whereas the anode hosts lithium in a charged cell. During battery operation, chemical potential is converted into electrical energy. The amount of energy that can be sourced is described by the capacity of the battery. As the battery ages its capacity diminishes due to several side-processes occurring within the battery cells, and significant research efforts are dedicated to better understand the ageing phenomena within the battery cells and ways of mitigating the degradation to develop longer-lasting batteries and reduce the waste associated with the battery industry.

Ageing Determination

LIB ageing stems mainly from the ageing of battery components – the individual cells. The ageing within cells is related to the degradation of its components, mainly the anode, cathode and electrolyte. The degradation mechanisms are based on several interconnected physical and chemical phenomena, which are yet to be explained and evaluated fully due to their complexity. The degradation within battery cells can be classified under two main outcomes – loss of lithium inventory (LLI, from electrolyte and electrodes) and loss of active material (LAM, from electrodes). Both are evident from the eventual loss of capacity during battery cycling. The various degradation phenomena, although mostly known, are not yet fully investigated and understood. However, they clearly lead to battery capacity fading, or deterioration of the state-of-health (SoH) during cycling.

The SoH at a given point in battery lifetime is determined by expressing the capacity of the battery at any cycle as percentage of the initial capacity of the battery. SoH is a useful parameter that shows how close to the end of life (EoL) a given battery is. The cycle when SoH reaches 80 % is generally accepted to be the EoL of a battery. However, such batteries can still give sufficient energy for second life applications such as stationary energy storage. The issue arises when a given battery's initial state is not known (for example, a battery from an electric vehicle (EV) from a scrapyard) and only the capacity of the given cycle can be determined by charging and discharging the battery. In such cases, a quick method to determine the SoH of a battery, which does not depend

on the battery's history, would be preferential. Thus, great effort has been dedicated to finding simple and fast methods for SoH estimation of LIBs [4]–[6].

Degradation of LIBs is a complex phenomenon, which involves several interdependent ageing mechanisms. However, although ageing mechanisms are various and different, many of them are reflected in the voltage hysteresis of the charge–discharge curve [7], [8] (Figure 1). Voltage hysteresis is the sum of the overpotentials of the charge and discharge curve at any given cycle. Overpotential is the difference between the open circuit voltage (OCV) and the operating voltage of the cell. Usually, during charge, the operating voltage is higher than the OCV (more energy is needed to charge the cell than is stored in it). In contrast, during discharge, it is lower (less energy is obtained from the cell than is stored in it). Overpotential represents the total energy dissipation during charging and discharging of the cell [9], [10]. Hence, as a battery cell ages and internal resistance grows, more energy is required to overcome it, and the overvoltage and voltage hysteresis grow.

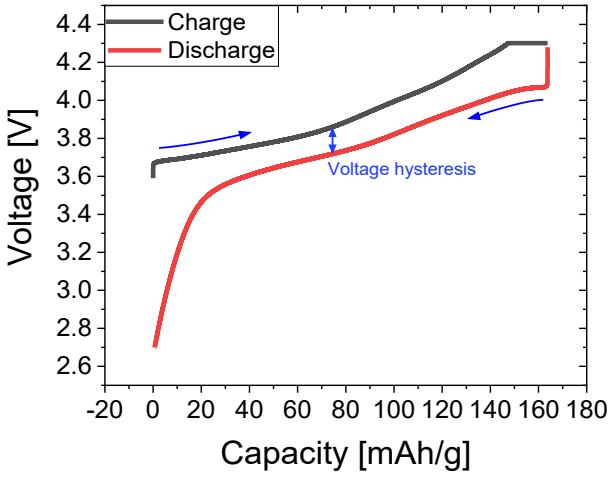

Figure 1. Voltage hysteresis of a typical charge–discharge curve of a LIB containing an NCM811 cathode.

The total overpotential is the sum of several smaller overpotentials originating from different resistances within the battery. These include charge transfer resistance due to activation energy of the charge transfer reactions at the electrode surfaces, lithium ion diffusion resistance in the electrolyte and in the bulk of the electrode materials, contact resistance between the different materials of the electrodes and current collectors, and ohmic resistance from electronic conductivity of the current collector and electrode active materials and ionic conductivity of the electrolyte [11].

Specific current j as a function of the voltage difference between the electrode and bulk electrolyte η (overpotential) is expressed by the Butler-Volmer (BV) equation:

$$j = j_0 \left[\exp\left(\frac{\alpha_a z F}{RT}\eta\right) - \exp\left(-\frac{\alpha_c z F}{RT}\eta\right)\right], \quad (1)$$

where j_0 – exchange current density, A/m^2;

α_a – anodic charge transfer coefficient, dimensionless;

α_c – cathodic charge transfer coefficient, dimensionless;

F – Faraday constant, C/mol;

R – universal gas constant, J/(K·mol);

z – number of electrons transferred in an electrochemical reaction;

T – temperature, K

η – overpotential.

The exchange current density is analogous to the rate constant used to describe the kinetics of chemical reactions, the anodic and cathodic charge transfer coefficients are kinetic parameters usually ranging from 0.2 to 2 and describe how much one direction of the electrochemical reaction is favoured over the other based on the applied potential, and for LIBs $z = 1$. The first and second terms in the parentheses of Equation (1) describe the rate of the anodic and cathodic reaction, respectively, and the difference in these rates gives the net rate of reaction at an electrode.

The way that the anodic and cathodic reactions overtake one another at positive and negative potential, respectively, can be clearly seen in the graphical depiction of the BV equation (Figure 2).

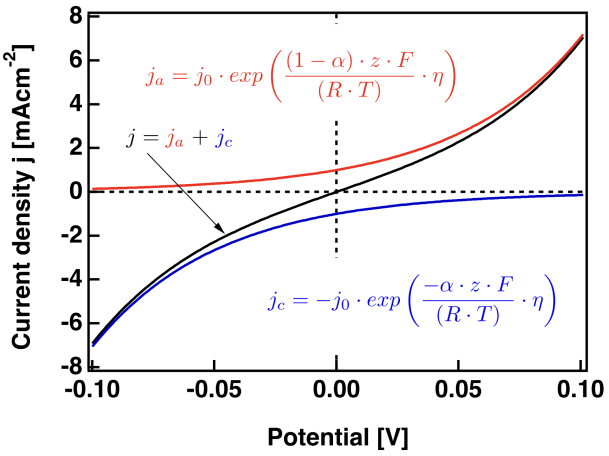

Figure 2. Graphical depiction of the Butler-Volmer equation [12].

When a LIB is charged, the cathode is delithiated, meaning that lithium is extracted from the lower energy, stronger bonding state in the cathode and inserted into the anode where it is bonded more weakly and has a higher energy. The Li^+ that exits the cathode has "lost an electron" (although the electron is lost by a transition metal (TM) in an oxide cathode for charge compensation purposes) in the process of oxidation, and the anodic current or reaction (red line in Figure 2) dominates the overall current. The opposite is true for the discharge or lithiation process (blue line in Figure 2).

The Doctoral Thesis attempts to utilise the relationship between the SoH and voltage hysteresis to establish a straightforward method for the determination of the SoH of a given battery based on a simple voltage hysteresis measurement – a task that usually requires storing large amounts of data and high computational power. The Doctoral Thesis tests the ability to determine the SoH from voltage hysteresis by fitting simple functions to the obtained data and calculating the error with which one could read the SoH value from the data plot if an unknown battery of the same composition was compared against it. Additionally, the SoH determination from one C rate measurement is explored as an alternative method.

NCM Cathode Degradation and Mitigation

The following sub-sections are based on the author's publication "A Review of the Degradation Mechanisms of NCM Cathodes and Corresponding Mitigation Strategies" [13][*]

Degradation

Cathode materials for rechargeable LIBs have been extensively studied for more than 30 years. Since the commercialization of LIBs, oxide cathode materials have been on the forefront of LIB cathode material research. Layered oxide cathode materials ($LiMO_2$, where M = Co, Ni, etc.), specifically $LiNi_xCo_yMn_{1-x-y}O_2$ (NCM) materials have gained significant popularity. NCMs are divided into low Ni-content NCMs ($x<0.8$) and high Ni content NCMs ($x\geq0.8$). Along with reducing the amount of cobalt in the material, research and industry strive for higher nickel content NCMs to achieve higher capacities. However, with the increased Ni content, NCMs suffer from exacerbated degradation.

The degradation mechanisms associated with the NCM cathode are illustrated in Figure 3. They primarily arise from two sources: the synthesis and handling of the cathode material and the operation of the battery (lithiation-delithiation of the cathode) once the cathode is integrated into the cell. Both aspects are examined in detail in the full version of the Doctoral Thesis; however, here focus is on the degradation occurring during battery operation. During synthesis it is crucial to control lithium content to prevent under-lithiation of the active material which can lead to subpar performance. However, when excess lithium is used in active material synthesis, it can remain on the particle surface and participate in the formation of residual lithium compounds (RLCs). RLCs can also grow during improper handling and storage of the NCM material, exposing it to air. RLCs

[*] The author's original publication.

lead to LLI in the assembled cell and participate in undesirable reactions with the electrolyte. Besides handling and storage, NCM undergoes the most critical and complex degradation during cycling.

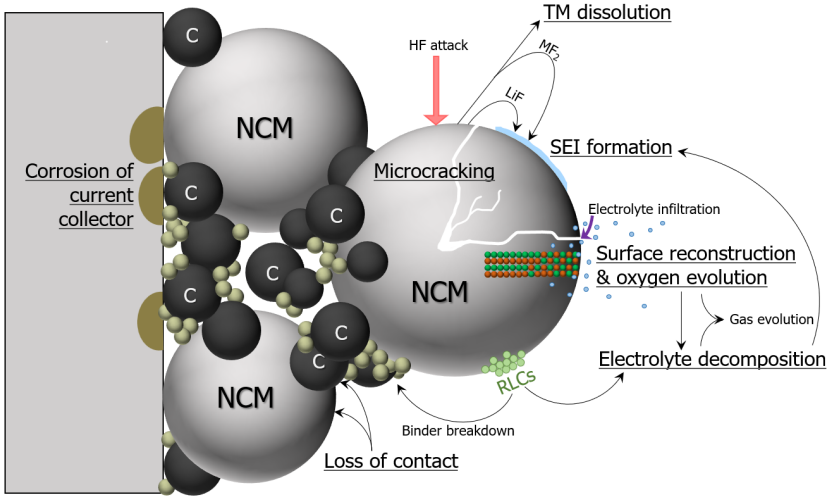

Figure 3. NCM cathode degradation mechanisms [13]*.

Key degradation mechanisms for any NCM cathode material during cycling include cathode-electrolyte interphase (CEI) formation, surface reconstruction, oxygen release, TM dissolution, and microcracking, creating new reactive surfaces. These degradation mechanisms are deeply interconnected and can be a trigger for further degradation outside of the cathode. The wide range of decomposition mechanisms (with some causing secondary degradation effects) and the variety of NCM compositions contribute to the challenges in fully understanding the relative contribution and significance of each degradation mechanism in quantifiable terms.

Identifying the most critical degradation mechanism in NCM cathodes would require a comprehensive investigation, in which individual phenomena, such as cation mixing, oxygen evolution, lattice collapse, microcrack formation, TM dissolution, and CEI formation, are isolated and their respective impacts on capacity, rate capability, and cycling stability are assessed. However, conducting such a study is nearly impossible, as these degradation processes are highly interconnected; the initiation of one mechanism often triggers or accelerates another, leading to a cascade of degradation effects.

The primary instabilities in the NCM cathode, and thus the onset of degradation, stem from disruptions in the $LiNi_xMn_yCo_zO_2$ stoichiometry, which occur when lithium is deintercalated from

* The author's original publication.

the cathode and migrates toward the anode during charging. For instance, oxygen evolution begins at approximately 80 % SoC due to excessive charge compensation by lattice oxygen following lithium extraction. This oxygen release depletes the lattice of oxygen, inducing phase transitions on the particle surfaces, which, in turn, exacerbate mechanical stress within the primary particles. The resulting intragranular microcracks hinder lithium-ion diffusion, ultimately reducing capacity, rate capability, and cycling stability. In this degradation sequence, lithium extraction beyond 80 % SoC acts as the initial trigger, yet it cannot be avoided if high capacity is to be achieved. The direct consequence of lithium removal is charge compensation by Ni and oxygen. This effect can be altered through various doping strategies which increase the effective charge of oxygen, helping it remain within the lattice and thereby mitigating oxygen evolution [14], [15]. Thus, in this chain of degradation effects, preserving lattice oxygen is crucial to reducing overall material instability.

Another example of degradation interplay is CEI formation, which arises from RLC species, dissolved TMs, and electrolyte decomposition products. In this scenario, mitigation efforts focus on removing RLC residues from the cathode surface post-synthesis, preventing TM dissolution, and limiting both oxygen evolution and direct electrolyte interaction. These objectives are typically achieved through post-synthesis washing of the cathode, doping strategies, or surface coatings on the active material.

In NCM cathodes with varying nickel content, the primary degradation mechanism is largely influenced by the extent of delithiation. As the nickel content increases, the critical SoC of 80 % is reached at lower voltages. Degradation in NCM cathodes is typically assessed based on the commonly applied upper voltage limit of 4.3 V vs. Li/Li+, which is selected considering the electrochemical stability window of both the electrolyte and cathode materials. When an NCM battery is charged to 4.3 V, the dominant degradation mechanisms shift from being predominantly surface-driven in NCM111 to bulk degradation playing a more significant role in NCM811, surpassing surface deterioration.

A comparison of the cycling stability of NCM111 and NCM811 reveals that the overall degradation of NCM811 occurs at a much faster rate than that of NCM111. However, with an increase in nickel content, a higher capacity can be achieved, which justifies the extensive efforts dedicated to enhancing the stability of high-nickel NCMs.

Mitigation

The sub-section is based on the author's publication "Wet-Chemical Synthesis of a Protective Coating on NCM111 Cathode: The Quantified Effects of Washing, Sintering and Coating" [16][*]

Various mitigation strategies have been proposed to address the degradation mechanisms in NCM cathodes. Wet-chemical coating is a preferred synthesis method due to its relative simplicity and time and cost efficiency, typically involving the dispersion of the active material in a solvent,

[*] The author's original publication.

the addition of a coating precursor, and a final sintering step to achieve the desired product [17]–[19].

Interestingly, sintering under conditions like those used for protective coatings has been shown to enhance electrochemical performance by promoting surface reconstruction and removing RLCs [3]. If the active material has been exposed to ambient conditions during delivery or processing, improvements in cycle life resulting from re-sintering and RLC removal might be mistakenly attributed to the protective coating. In fact, many wet-chemical coating studies compare only pristine and coated materials, often attributing all observed stability and capacity enhancements solely to the coating itself [17], [19], [20]. The extent to which washing and sintering influence the active material during this type of processing remains uncertain [21], [22].

There is an abundance of coating studies exploring different wet-chemical coatings on NCM materials, most of which show promising results with improved cycling stability and capacity [17], [23]. However, many of these studies use untreated commercial NCM materials as references, and attribute all capacity and stability improvements to the coating effects [20], [24]–[26], when some improvements might be due to the coating procedure itself (washing and sintering the material).

To accurately assess the role of the inert protective coating, this study not only compares the electrochemical performance of coated and uncoated NCM but also systematically examines the individual and combined effects of washing and sintering on capacity retention. In addition to evaluating electrochemical behaviour, surface chemistry analysis and carbon quantification are conducted to identify compositional changes in the active material. This comprehensive approach ensures that improvements in cycle life are properly attributed to washing, sintering, and coating steps, rather than being misinterpreted as solely coating-induced.

Meta-analysis of NCM Cathode Coating vs. Doping

The following sub-section is based on the author's publication "A Review of the Degradation Mechanisms of NCM Cathodes and Corresponding Mitigation Strategies" [13][*]

An analysis of the available research literature reveals a vast collection of electrochemical data obtained under a wide range of experimental conditions. However, the significant variability in parameters, such as particle size and morphology, electrode composition, electrolyte type, voltage range and corresponding SoC, temperature, and applied specific current, makes direct comparisons between individual studies challenging. This variability complicates the ability to draw definitive conclusions unless a comprehensive, systematically controlled study is conducted.

Despite these limitations, when examined collectively, certain trends emerge that allow for broader analysis without requiring a direct focus on the specific conditions of individual studies. While data remains somewhat scarce, notable tendencies in the effectiveness of doping versus surface coating as a function of Ni content in NCM cathodes can be identified. Figure 4 compiles findings from 45 studies, quantifying the extent to which doping or surface coating has enhanced

[*] The author's original publication.

the cycle life of pristine NCM111, NCM622, and NCM811. Given that many studies limit their cycle life assessments to only 50 or 100 cycles, two graphs illustrate capacity retention at these benchmarks (Figure 4). The improvement in capacity retention on the vertical axis is expressed in percentage points (%CR), calculated based on the additional capacity retained in the 50th or 100th cycle of the treated material ($CR_{\text{treated NCM}}$) compared to the reference material in each study ($CR_{\text{reference NCM}}$):

$$\%CR = \frac{CR_{\text{treated NCM}} - CR_{\text{reference NCM}}}{CR_{\text{reference NCM}}}, \quad (2)$$

where $CR_{\text{treated NCM}}$ – improvement in capacity retention of the treated material, %;

$CR_{\text{reference NCM}}$ – improvement in capacity retention of the reference material, %.

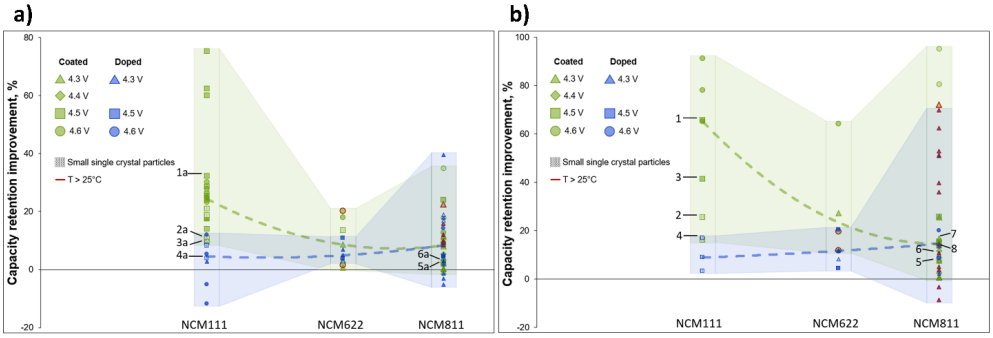

Figure 4. Capacity retention improvement (calculated as shown in Equation (2)) after a) 50 cycles and b) 100 cycles of coated and doped NCM cathodes compared to the reference untreated samples as reported in 45 literature sources [13]*.

Since the absolute cycle life of reference (pristine) materials varies significantly, relative improvements are compared instead of absolute values. While the complexity of such a dataset remains, a detailed data table is available in the supplementary information of the original publication for those interested in drawing their own conclusions.

For NCM111, the trends are relatively clear – statistically, surface coating provides a more significant enhancement in cycle life compared to doping. As the SoC (or degree of delithiation) remains relatively low within the same voltage range, and lattice parameter changes are minimal, NCM111 exhibits little to no microcracking. As a result, doping strategies aimed at mitigating lattice strain are less effective in extending cycle life. Instead, surface protection proves more beneficial in reducing degradation, as degradation in NCM111 occurs more prominently at the surface rather than within the bulk.

In the case of NCM622, the evolution of SoC with voltage closely resembles that of NCM111 [27]; however, the critical SoC at which lattice parameter variations become significant

* The author's original publication.

is reached at a slightly lower voltage. Consequently, a combination of doping and surface coating is the most effective strategy for improving the cycle life of NCM622.

For NCM811, a higher SoC is reached at lower voltages, leading to more pronounced lattice parameter changes. In this case, doping plays a crucial role in mitigating bulk degradation. However, to achieve optimal cycle life improvements, surface coating should also be implemented to counteract surface degradation and electrolyte decomposition.

From Figure 4 it can be inferred that for Ni-rich NCMs the optimal strategy for mitigating degradation is a combination of coating and doping. Furthermore, structural control of the particles could bring additional improvements, however, a more extensive study would need to be conducted.

NCM materials are derived from layered oxide cathode materials and have progressively evolved toward higher nickel content. This shift has been driven by the need to enhance energy density and address some of the sustainability concerns associated with these materials. However, as the nickel content increases, various stability-related challenges emerge. A comprehensive review of the literature indicates (Figure 4) that the dominant aging mechanisms vary depending on the Ni content, implying that the most effective mitigation strategies for NCM degradation should be tailored according to Ni stoichiometry.

An analysis of the effects of coating and doping on NCM degradation mitigation across different Ni compositions reveals distinct trends, as summarised in Table 1. With an increase in Ni content and a corresponding reduction in the voltage at which a critical SoC is reached, the importance of stabilising the crystal lattice and mitigating volume changes through doping becomes more pronounced. In NCM111, where degradation is primarily surface-related, coating proves significantly more effective in enhancing performance compared to doping. In NCM622, the emergence of microcracks as a key degradation factor necessitates doping to stabilise the cathode structure, making it comparatively more effective in degradation mitigation. For NCM811, where structural instabilities become more severe, doping and coating are equally important in ensuring long-term stability. When Ni content exceeds 80 %, both doping (to counteract the more significant lattice parameter changes occurring at lower lithium content) and coating (to prevent rapid surface degradation) should be strongly considered due to the accelerated degradation rate and the increased complexity of degradation pathways [28].

Table 1

Summary of Degradation Mechanisms for Various NCM Materials and Corresponding Mitigation Strategies [13][*]

Composition	Degradation	Mitigation
NCM111	Cation mixing, surface reconstruction, oxygen release, RLCs, CEI formation	On average, coating strategy is superior to doping
NCM622	Cation mixing, surface reconstruction, oxygen release, RLCs, CEI formation, microcracking	Coating provides more significant improvement; doping strategies also notably improve performance
NCM811	Cation mixing, surface reconstruction, oxygen release, RLCs, CEI formation, significant microcracking	Coating and doping strategies provide comparable improvement to capacity retention

Materials and Methods

Coating Synthesis

Al_2O_3 Coated Samples

The coatings were synthesized on the surface of NCM111 and NCM811 (*MTI corp.*) cathode active materials (CAMs) by a wet-chemical method. For $LiAlO_2$/Al_2O_3 coating a certain amount of aluminum isopropoxide or AIP (*Sigma Aldrich*, ≥ 98 %) was dissolved in ethanol (99.8 %) within 20–30 minutes under light heating (up to 50 °C) after which the heating was removed and NCM powder added to the mixture. The weight of AIP was chosen so that the resulting Al_2O_3 coating would account for roughly 3 wt% of the coated NCM, and the volume of ethanol was chosen accordingly (for example, to coat 3 g of CAM 0.3716 g of AIP were dissolved in 20 mL of ethanol). After 30 minutes of stirring and dispersing the CAM, a stoichiometric amount of H_2O (ultrapure, type 1 water, > 18 MΩ/Cm obtained from *Direct-Q R & Direct-Q UV-R* water purification system) was added to the mixture in the form of an ethanol-H_2O (95:5 volume ratio) solution. Thereafter, the solution was stirred for 2 more hours to allow coordination of the -OH groups of the formed $Al(OH)_3$ to the oxygen groups on the surface of NCM. The mixture was subsequently centrifugated at 2000 rpm and 6000 rpm for 7 minutes each using a *Hermle Z 306* tabletop centrifuge and washed with ethanol twice before transferring to a crucible to dry overnight at 80 °C. The next day the dried powder was sintered at 500 °C for 4 h in air using *Nabertherm L*

[*] The author's original publication.

9/13 high temperature furnace, after which it was potted and stored in a glove box in Ar atmosphere with H_2O and O_2 levels <0.5 ppm.

Reference Samples

Since coating synthesis involves several steps which could also affect the material properties, a proper reference sample was synthesized by following all the steps of the coating procedure, but without the addition of AIP and H_2O (NCM was stirred for 2.5 h in ethanol, centrifugated and washed twice, dried at 80 °C overnight, and sintered at 500 °C for 4 h in air).

Furthermore, two more samples were prepared to assess the effect of washing and sintering separately on the properties of the CAM. The sample assessing washing was prepared by stirring the CAM for 2.5 h in ethanol, centrifugating and washing it twice with ethanol, then drying under vacuum at 80 °C overnight. The sample for the assessment of the effects of sintering was prepared by sintering the CAM at 500 °C for 4 h in air.

Electrode Preparation

Magnetic Stirring and Ultrasonication

For the coated samples and respective reference samples magnetic stirring and subsequent ultrasonication were used to create electrode slurries. In a 50 mL beaker 5 wt.% polyvinylidene fluoride or PVDF (powder, *Sigma Aldrich*, ≥ 99.5 %) solution in N-methyl-2-pyrrolidone or NMP (*Sigma Aldrich*, anhydrous, 99.5 %), CAM (coated, uncoated NCM111, or reference samples), and carbon black (*Alfa Aesar*, 99.9+ %) were weighed in a proportion CAM : carbon : PVDF = 75:15:10. The slurry was mixed by magnetic stirring for 2 h at 400 rpm, then treated in an ultrasound bath (*Elmasonic S 120 (H)*, 37 kHz) for 30 min, and stirred again for 30 min.

Ball Milling

For the LIB ageing determination experiments, electrode slurries were prepared by ball milling. The electrode components were weighed into a stainless-steel ball mill container in a proportion CAM : carbon : PVDF = 75 : 15 : 10, with PVDF in the form of a 5 % (by weight) solution in NMP. The CAM used in these experiments was NCM811. The slurries were ball-milled (*Retsch MM200*) at 15 Hz for 60 min.

Electrode Coating and Drying

The prepared slurries were coated onto an Al foil (*Sigma Aldrich*, 0.015 mm thickness) by a typical tape casting method. Al foil was attached to a glass plate (10 cm × 10 cm), then a pool of electrode slurry was deposited on one end of the glass plate in the middle. Using a *Dr. Blade* coating instrument (± 5 µm) the electrode slurry was evened out (starting at 500 µm down to 100 µm in increments of 100 µm) by dragging the instrument over the pool of slurry and the whole Al-covered glass plate until a broad line of electrode slurry with a wet thickness of 100 µm was obtained. The prepared electrode sheets were then properly marked and put into a vacuum oven (*Shanghai Yuanhuai Industrial Co., Ltd., DZF-6020*) to dry at 80 °C under vacuum overnight.

Electrode Punching and Weighing

Electrodes with a diameter of 10 mm were punched out from the dried electrode sheets using a manual electrode disc cutter (*TOB New Energy TOB-CP60*). The obtained electrode discs were subsequently weighed on an analytical-grade laboratory scale (*Kern, ABT 120-5DNM, ± 0.001 mg*). To calculate the weight of the active material in one electrode, an Al foil disc of the same dimensions was cut out, and its weight was subtracted from the weight of the whole electrode. Afterwards, 75 % of the remaining weight was calculated as the CAM mass.

Cell Assembly

Coin Cells

All electrochemical tests for the coating experiments (with NCM111) and LIB ageing experiments (with NCM811) were carried out in coin cells (CR2032 stainless steel grade 316L, *Xiamen Tob New Energy Technology Co., Ltd.*). The coin cells were assembled in an Ar-filled glove box (*M. Braun Inertgas-Systeme GmbH, EASYlab workstation*) with H_2O and O_2 levels < 0.5 ppm. A spring was inserted into the battery casing, then Li foil (*Alfa Aesar*, 1.5 mm thickness, ≥ 99.9 %) was thoroughly scraped to clean off any reacted lithium from both sides. Negative electrode (11.1 mm in diameter) was then punched from the cleaned lithium foil and pressed to a spacer, which was then stacked on top of the spring. Then, a *Whatman* GF/B glass fiber separator was punched (15.8 mm in diameter) and positioned on the Li electrode, after which 200 µL of electrolyte ($LiPF_6$ solution in EC/DEC, 1:1 volume ratio, with 5 % fluoroethylene carbonate or FEC additive for the LIB ageing study and without FEC for the coating study) was added onto the separator using a micropipette. The prepared cathode was positioned onto the electrolyte-soaked separator using clean Teflon-coated plastic tweezers. The coin cell was closed with a lid and pressed together using a hydraulic coin cell press (*TOB Machine, TOB-MR-120*). All components of the coin cell stack were centered to avoid any short circuits or displacement of lithium foil against the cathode. The assembled coin cells were marked appropriately for further electrochemical testing.

Structural Characterisation

All sample CAM powders for the coating study were characterised using X-ray diffraction (*Rigaku Miniflex 600*, Cu $K\alpha_{1,2}$), X-ray photoelectron spectroscopy (*ThermoFisher ESCALAB Xi+* with a monochromatic Al Kα X-ray source), scanning electron microscopy (*Thermo Fisher Scientific Helios 5 UX*) with energy-dispersive X-ray spectroscopy (EDS), transmission electron microscopy (*Fei Tecnai*) with EDS (*EDAX*), inductively coupled plasma mass spectrometry (*Agilent Technologies 8900 ICP-QQQ*), and isotope ratio mass spectrometry (*Nu Horizon* in conjunction with elemental analyzer *EuroVector Euro EA3000*) methods.

Electrochemical Characterisation

All rate capability and cyclability measurements were carried out in half-cells (containing metallic lithium anode) using a *Neware BTS-4000* series battery tester at a controlled 25.0 ± 0.1 °C temperature (*Neware MHW-25-S* constant temperature chamber).

Rate Capability and Cyclability for SoH Estimation Studies

To electrochemically test the NCM811 active material during the SoH estimation studies, 17 cells were cycled in two different modes (two series of cells) to observe if the cycling mode would influence the evolution of voltage hysteresis in relation to SoH.

1. The following steps were repeated on a loop until SoH dropped to at least 80 %:
    - rate capability – five charge–discharge cycles at specific currents ranging from 0.1 C to 10 C (0.1 C, 0.2 C, 0.5 C, 1 C, 2 C, 5 C, 10 C);
    - cycling – 100 charge–discharge cycles at a specific current of 1 C.
2. The following steps were carried out:
    - initial rate capability – five charge-discharge cycles at specific currents ranging from 0.1 C up to 10 C (0.1 C, 0.2 C, 0.5 C, 1 C, 2 C, 5 C, 10 C);
    - cycling – charge-discharge cycling at a specific current of 1 C until SoH drops to at least 80 %;
    - final rate capability – five charge–discharge cycles at specific currents ranging from 0.1 C up to 10 C (0.1 C, 0.2 C, 0.5 C, 1 C, 2 C, 5 C, 10 C).

1 C (200 mA/g for NCM811) corresponds to the specific current required to charge or discharge the battery cell in one hour. The value depends on the theoretical specific capacity (200 mAh/g).

The cells were cycled using constant current, constant voltage (CCCV) charging and constant current (CC) discharging mode in the range from 2.7 V to 4.3 V vs. Li/Li^+. The cut-off current for the constant voltage step was 10 % of the CC charging current.

Rate Capability and Cyclability for Coating Studies

For the coating studies on NCM111, active material rate capability testing was carried out in separate cells from cycling stability measurements.

- Rate capability – five charge–discharge cycles at specific currents ranging from 0.1 C up to 20 C (0.1 C, 0.2 C, 0.5 C, 1 C, 2 C, 5 C, 10 C, 20 C).
- Cycling stability – 500 charge–discharge cycles at a specific current of 1 C.

1 C for NCM111 corresponds to 170 mA/g. The cells were cycled using CC charging and discharging in the voltage range of 2.7–4.3 V vs. Li/Li^+.

For the coating studies on NCM811 material, the testing was performed differently from coating studies on NCM111.

- Cycling stability – three formation cycles at a specific current of 0.1 C followed by 500 charge–discharge cycles at a specific current of 1 C.

The cells were cycled using CCCV charging and CC discharging modes in the range from 2.5 V to 4.3 V vs. Li/Li^+. The cut-off current for the constant voltage step was 10 % of the CC charging current.

Data Processing

Charge–Discharge Measurements

Current and time are used to calculate the capacity of the cell during charging and discharging by the formula:

$$Q_0 = I \times t, \tag{3}$$

where I – current, mA;

t – time, h.

Since the mass of the electrode is known, the mass of the active material can be calculated by the following equation:

$$m_{\mathrm{AM}} = (m_{\mathrm{el}} - m_{\mathrm{cc}}) \times r, \tag{4}$$

where m_{el} – mass of the whole electrode, g;

m_{cc} – mass of the current collector, g;

r – ratio of the active material in the electrode, between 0 and 1, dimensionless.

In the scope of the research, r from Equation (2.2) corresponds to 0.75 (other parts are composed of binder and conductive additive).

Using Q_0 and m_{AM}, we can calculate the specific capacity or gravimetric capacity, which is the capacity normalized by the active material mass:

$$Q = \frac{Q_0}{m_{\mathrm{AM}}}. \tag{5}$$

Another important measure of the performance of the battery cell is the Coulombic efficiency (CE):

$$CE = \frac{Q_{\mathrm{disch}}}{Q_{\mathrm{ch}}} \times 100\%, \tag{6}$$

where Q_{disch} – discharge capacity, Ah;

Q_{ch} – charge capacity, Ah.

The Coulombic efficiency describes the loss of charge in each charge–discharge cycle, directly related to the loss of lithium.

State of Health (SoH) and State of Charge (SoC)

The state of health (SoH) is calculated at any point during the cell's lifetime using the following formula:

$$SoH = \frac{Q_n}{Q_{\mathrm{i}}}, \tag{7}$$

where Q_n – capacity at any given cycle, Ah;

Q_{i} – initial capacity, Ah.

Usually, the end of a cell's lifetime or EoL is considered when SoH has reached 80 %.

The state of charge (SoC) is calculated from the specific capacity (or capacity) in each cycle from the charge–discharge curve, with 0 % SoC corresponding to a completely discharged cell (fully lithiated cathode) and 100 % SoC corresponding to a completely charged cell (delithiated cathode).

$$\mathrm{SoC} = \frac{Q_x}{Q_n}, \tag{8}$$

where Q_x – capacity (or specific capacity) at any given point during charging or discharging the cell, Ah;

Q_n – full capacity (or specific capacity) of the cycle from which Q_x is obtained, Ah.

Determination of voltage hysteresis at certain SoC is described in more detail in the result section regarding SoH estimation studies.

Results and Discussion

State of Health Estimation from Voltage Hysteresis

The section is based on the author's publication "State of Health as a Function of Voltage Hysteresis in Li-Ion Battery Half-Cells" [29][*].

Voltage Hysteresis Determination and Significance

Voltage hysteresis is the sum of overpotentials when charging and discharging a battery cell. As the battery ages during charge–discharge cycling, its internal resistances increase, which is indirectly depicted in the rise of voltage hysteresis. Additionally, voltage hysteresis increases with specific current, as stated by the Butler-Volmer equation (Equation (1)); hence, the SoH evolution with ageing is different at each specific current. The SoH dependency on voltage hysteresis is characterised at specific currents up to 5 C.

The employed measurement and data acquisition procedure is depicted in Figure 5. Charge–discharge cycling at 1 C rate was combined with rate capability measurements every 100 cycles (Figure 5a). The 80 % SoH value corresponding to the EoL was reached already after 100 cycles; however, for more elaborate analysis, the cells were cycled further until about 53 % SoH.

The voltage hysteresis value at 50 % SoC at each C rate was obtained as shown in Figure 5b. 50 % SoC was calculated based on the capacity obtained in each cycle. Figure 5c clearly depicts the growth of voltage hysteresis with increasing C rate in a manner similar to Butler-Volmer curve. These curves at certain SoHs are the main sources of information used for further analysis of the

[*] The author's original publication.

relationship between SoH and voltage hysteresis, and for developing ways to determine SoH based on the value of the voltage hysteresis.

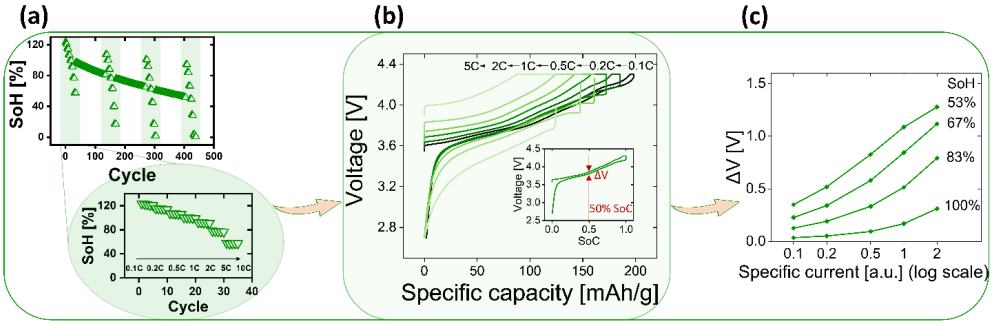

Figure 5. Illustration of voltage hysteresis determination from charge–discharge curves (a–b) and voltage hysteresis growth with increasing applied specific current and decreasing SoH (c) [29]*.

SoH Determination from Voltage Hysteresis

The positive correlation between voltage hysteresis and battery ageing is consistent among all 17 cells measured (Figure 6a), independently of the measuring regime used (with or without intermittent C rate measurements). From the voltage hysteresis growth tendency in Figure 6a, one can observe that at the same SoH the voltage hysteresis is larger for cells cycled at higher C rates than those cycled at lower C rates. This growth in hysteresis has a purely kinetic origin from the higher charge-discharge rate and not because the battery ageing is more advanced. As the rate capability measurements (from which the voltage hysteresis vs. SoH data was obtained) are carried out only every 100 cycles, there is a lack of data points between 100 % and 80 % SoH already reached after 100 cycles. However, the remaining measurements beyond 80 % SoH allow finding functions that best describe this relationship (Figure 6 and Table 2).

* The author's original publication.

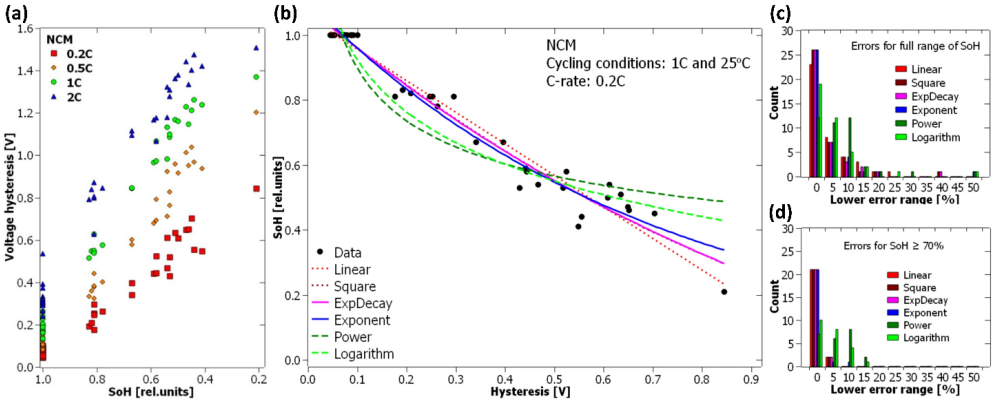

Figure 6. Voltage hysteresis increase with SoH at different C rates (a), SoH as a function of voltage hysteresis at 0.2 C rate fitted by various basic functions (b), error distribution of the different fit functions for the whole SoH range (c) and for SoH ≥ 70 % (d)[29]*.

The increase in voltage hysteresis with diminishing SoH in Figure 6a can be flipped to allow reading the SoH from voltage hysteresis (Figure 6b, data obtained from 0.2 C rate measurements). This relationship (SoH = f(ΔV)) could allow determining the SoH of NCM-Li cells at any given point in battery life with a certain error, if a function describing this relationship could be determined. In Figure 6b, the data is fit by several basic functions for which the parameter errors and coefficients of determination R^2 are calculated (Table 2) to evaluate the best fit. Consequently, logarithm and power functions are discarded as possible fits.

Linear, exponential, square, and exponential decay approximations provide the best fit for the full range of SoH, achieving R^2 values above 0.996 and maintaining the highest error count below 5 % (Figure 6c). However, the parameter errors for the square and exponential decay functions are too large (up to 102 %, Table 2), making them unsuitable for SoH determination. When evaluating the remaining linear and exponential functions at SoH levels above 70 %, only the exponential function exhibits errors exceeding 5 %, with a single instance reaching 10 % (Figure 6d). Consequently, linear and, to some extent, exponential functions serve as the most precise approximations for SoH determination from voltage hysteresis. The linear function fits well above 70 % SoH, whereas the exponential function more accurately represents the accelerated battery ageing below this threshold. Additionally, if the ΔV value is derived from a single charge–discharge measurement of an NCM811 half-cell and compared with the linear function down to 70 % SoH, SoH determination from this ΔV value could achieve 5 % accuracy.

* The author's original publication.

Table 2

Basic Approximation Function Coefficients with Relative Errors Indicated in the Parentheses, and Coefficients of Determination R^2 for Half-Cells Containing NCM811 Electrodes [29]*

Function	Coefficient			R^2
	*a*0	*a*1	*a*2	
ExpDecay $a0+a1*\exp(-x/a2)$	–0.459 +/– 0.469 (102 %)	1.544 +/– 0.458 (30 %)	1.182 +/– 0.345 (29 %)	0.997230
Square $a0+a1\times x+a2\times x^2$	1.081 +/– 0.0158 (1 %)	–1.240 +/– 0.115 (9 %)	0.372 +/– 0.154 (41 %)	0.997202
Exponent $y=a0\times\exp(a1\times x)$	1.104 +/– 0.014 (1 %)	–1.403 +/– 0.050 (4 %)	-	0.997052
Linear $a0+a1\times x$	1.054 +/– 0.012 (1 %)	–0.973 +/– 0.031 (3 %)	-	0.996761
Logarithm $y=a0+a1\times\ln(x)$	0.389 +/– 0.022 (6 %)	–0.232 +/– 0.012 (5 %)	-	0.992461
Power $y=a0\times x^a1$	0.464 +/– 0.021 (5 %)	–0.287 +/– 0.020 (7 %)	-	0.988315

In a battery cell with two electrodes, the BV equation (Equation (1)) can be used to describe each electrode operation individually. Although lithium as a counter electrode has often been regarded as the perfect anode and used in half-cells to study other LIB electrodes without considering the contributions from the Li metal electrode, it has been shown that it does contribute to the overpotential rise in full cells [30]. Nevertheless, by only considering the cathode contribution to the total overpotential in a battery cell and by assuming the anodic charge transfer coefficient α_a to be 0 during the charge and the cathodic charge transfer coefficient α_c to be 0 during the discharge of the cell (neglecting the counterpart of the net reaction at the cathode), the correlation between the specific current and voltage hysteresis has been fitted with a BV-like equation (Equation (9)) at different states of health (SoH), discussed further in the publication [29]*.

* The author's original publication.

$$y = a(e^{bx} - 1), \tag{9}$$

where a, b – fitted parameters, dimensionless;

x – voltage hysteresis, V.

While introducing these simplifications holds no electrochemical meaning, it does provide a good approximation of the three-way relationship between voltage hysteresis, specific current and SoH and an additional method of determining the SoH of a cell based on the observed voltage hysteresis at different specific currents (Figure 7). Additionally, the same equation was used to fit the specific current vs. voltage hysteresis at different SoHs for $LiFePO_4$ (LFP) half-cells [29]*, thus suggesting that it could be used for multiple cathode chemistries.

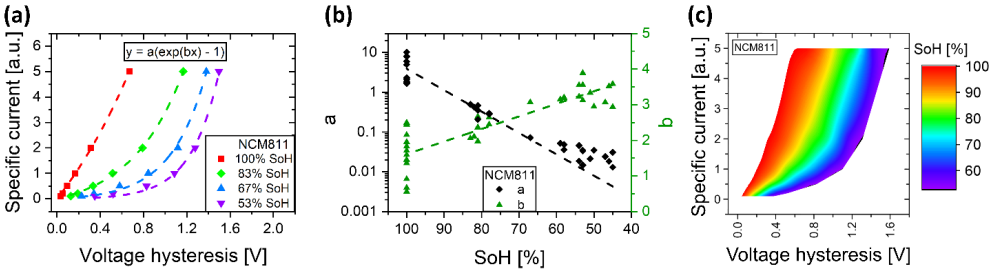

Figure 7. Specific current as a function of voltage hysteresis approximated by a BV-derived equation (a), the respective a and b equation parameter dependency on the SoH of the NCM811 half-cell (b). A visualisation of SoH determination from the voltage hysteresis measurements at different specific currents (c), data obtained from seven cells [29]*.

Although the simplified BV-derived fit in Figure 7a does not describe the electrochemistry of the cell, it very closely approximates ($R^2 \geq 0.99$) the relationship between specific current (or C rate) and voltage hysteresis, which does stem from the principles of the BV equation. While hysteresis at near-zero current is not always zero [31], [32], and charge–discharge reactions can display asymmetry [33] with lithiation and delithiation processes being inhomogeneous across the electrode [34], the proposed method offers an initial, yet valuable insight.

The selected approximation function aligns well with the obtained data points and passes through the origin (0,0), satisfying the theoretical requirements of the BV function (Figure 7a). The fit parameters, a and b, of the BV-derived function (Equation (9)) were estimated using simple exponential and linear functions, respectively (Figure 7b). Despite some dispersion, these parameters exhibit consistent trends as SoH declines – parameter a decreases exponentially, while b increases linearly. To ensure more comparable fit parameters, certain data points approaching the

* The author's original publication.

maximum possible voltage hysteresis based on the measurement voltage range (1.6 V) were excluded from the fit.

The fitted data from multiple half-cells, as shown in Figure 7a, can be combined to demonstrate how voltage hysteresis evolves with increasing C rate and decreasing SoH (Figure 7c). In this representation, data from seven NCM811-containing half-cells were merged into a 3D plot, illustrating the general SoH regions associated with varying specific currents and corresponding voltage hysteresis. This visualisation could serve as a reference for SoH estimation using a single rate capability measurement ranging from 0.1 to 5 C. By approximating the obtained C rate and voltage hysteresis data with a BV-like function, it can then be compared against the SoH visualisation graph (Figure 7c). The described approach, however, requires somewhat advanced data analysis. Thus, the direct SoH vs. voltage hysteresis comparison at a certain C rate (Figure 6) gives a quicker, easier and more direct way of estimating the SoH.

Summary: SoH Determination Limitations and Prospects

Following the need for easier and more direct ways to determine the SoH of a given battery, it has been demonstrated how the SoH can be estimated either from the voltage hystereses of one rate capability measurement and fitting a BV-derived equation (Equation (9)) to the data or from the voltage hysteresis measurement of one charge–discharge cycle and reading the SoH value from a fitted graph. Admittedly, the proposed method is based on very specific parameters (cathode, anode chemistry, and measurement setup). However, it can serve as a guide or a building block for a detection system that can determine the SoH of a given battery based on one charge–discharge measurement with a certain error, thus allowing the batteries from scrap yards and recycling stations to be utilised further in second life applications, avoiding premature recycling.

The relationship between SoH and voltage hysteresis for NCM811 half-cells at 0.2 C can best be fit by a linear approximation for SoH values above 70 %; however, below 70 %, the relationship is more accurately described by an exponential function. By combining these two fits at the appropriate SoH ranges, the SoH and voltage hysteresis relationship has been described down to around 20 % SoH. Below 20 % SoH one can argue that recycling the materials is justified.

It has also been shown that the relationship between the C rate and voltage hysteresis can be rather accurately fit by a simplified BV-derived equation (Equation (9)). This opens the possibility of exploring the SoH and voltage hysteresis relationship at different C rates, thus providing another way to estimate the SoH of an unknown battery, using the voltage hysteresis measurements at different C rates, rather than one definite C rate (which is usually not known for batteries of unknown loading). Hence, if the voltage hysteresis data at different C rates is fit by the BV-derived function, it can be compared against the constructed graph, and the SoH value can be found.

As mentioned before, the main limitations of the proposed methods include the demonstrated fits only being applicable to the chosen set of parameters (cathode, anode, electrolyte chemistry, other measurement parameters, which influence voltage hysteresis, such as temperature). This means that a common method or device for SoH estimation of any unknown battery would require

this kind of fitting to be done for each separate set of parameters. However, these findings present an intriguing avenue for future research.

Additionally, while a full range charge–discharge cycling has been conducted, it is important to note that a complete cycle may not always accurately reflect real-life applications or even be necessary. Instead, SoH estimation could rely on data from battery operation or targeted charging and discharging experiments within a narrower SoC range (for example, 40–60 % SoC). As expected, our results exhibit significant dispersion for half-cells assembled in laboratory coin-cell cases [35]. However, the ability to determine SoH with approximately 5 % accuracy, even in lab-built cells, suggests that mass-produced battery cells could demonstrate an even stronger correlation between voltage hysteresis and SoH.

Finally, it is important to highlight that this study focuses solely on half-cells with NCM811 cathodes, where LAM is the primary aging mechanism. However, the degradation process in full LIB cells is more complex.

NCM111 Ageing Mitigation

The section is based on the author's publication "Wet-Chemical Synthesis of a Protective Coating on NCM111 Cathode: The Quantified Effects of Washing, Sintering and Coating" [16][*].

While aging in LIBs consists of multiple phenomena, often a key player in performance degradation is the cathode. Additionally, many of the cathode aging processes promote anode and electrolyte degradation, and vice versa. Thus, protecting the cathode from degradation will enhance the overall stability of the battery cell.

Based on the meta-analysis drawn from several coating studies on NCM materials with different Ni content (see *Theoretical Background*), forming a protective coating on the active material to mitigate reactions with the electrolyte, transition metal dissolution, and oxygen evolution is a necessary step for improving the capacity retention of any Ni content NCM. However, for higher Ni content NCMs doping becomes an equally important if not more important strategy to prevent ageing of the material due to extensive microcracking that occurs as the material is delithiated beyond 80 %, which occurs at lower voltages for the higher Ni content NCMs (4.3 V vs. Li/Li^+) than for lower Ni content NCMs (4.6 V vs. Li/Li^+).

Although doping strategies are important in degradation mitigation, this study focuses on forming a protective coating on NCM material with 33 % and 80 % Ni content – NCM111 and NCM811, respectively. More specifically, a wet-chemical Al_2O_3 coating synthesis is developed on the surface of NCM materials. The coating synthesis is based on hydrogen bond formation between the hydrolyzed aluminum precursor and oxygen groups on the NCM particle surface (Figure 8). After the initial $Al(OH)_3$ layer is formed, the material is sintered in air at 500 °C to form the final Al_2O_3 coating.

[*] The author's original publication.

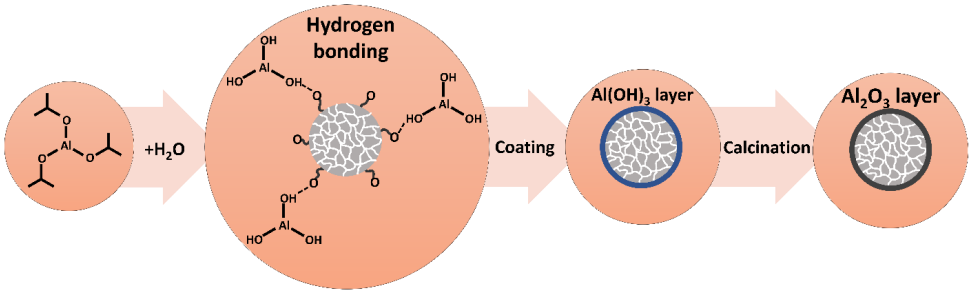

Figure 8. Wet-chemical Al_2O_3 coating process.

Wet-Chemical Coating on NCM111 Material

Washing and sintering are essential steps in all wet-chemical coating synthesis processes for electrode materials. Typically, the coating precursor is mixed with the electrode active material in suspension, then dried and sintered. The coated material is then compared to the uncoated material, with any improvements in electrochemical performance often attributed solely to the coating. However, while proper coating of cathode active materials can enhance electrochemical performance, significant improvements may also result from washing and sintering alone, as highlighted in the introduction. This is particularly true if the source material was improperly stored, leading to surface contamination, cation mixing, and a surface layered-to-spinel phase transition. To isolate the specific effects of the coating itself, this study eliminates the influence of washing and sintering by comparing the electrochemical performance of the coated material with that of a reference sample that has undergone the washing and sintering steps of the coating procedure.

Since washing, sintering, and coating alter the surface of the active material, the electrode preparation method must be carefully adjusted not to damage the surface coating or break apart the particles. Intensive mixing methods, such as wet ball milling or high shear processing, can fracture secondary active material particles, thereby revealing uncoated surfaces from within the particle bulk. This can obscure the stability improvements provided by surface coatings, as the newly exposed, uncoated surfaces may degrade. Additionally, while these methods enhance electrode homogeneity, ball milling has been shown to compromise particle integrity, negatively affecting electrochemical performance [36]. To preserve particle structure while ensuring electrode uniformity, a gentler approach has been chosen, using magnetic stirring followed by sonication at a frequency low enough (37 kHz) to preserve the secondary particles. This method allows for a direct comparison between pristine, coated, and reference materials – something that may not be feasible with more aggressive, energy-intensive mixing techniques.

Material Characterisation

Analysing the X-ray diffraction (XRD) results (Figure 9) for pristine, reference, and coated NCM111, no new phases are detected in the modified samples, suggesting that the coating is either

thin or amorphous. Similarly, no structural changes are observed in the samples that underwent only sintering or only washing. The *a* lattice parameter remains stable at approximately 2.8618 Å across all modifications, while the *c* lattice parameter (14.2373 Å) exhibits a minimal increase of less than 0.001 Å in reference and coated materials. These lattice parameters align well with previously reported values [37], [38].

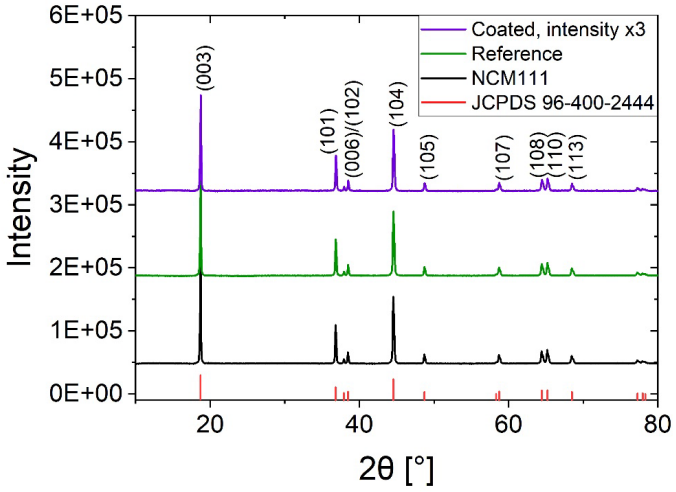

Figure 9. XRD analysis of pristine, reference, and coated NCM111 material [16]*.

Scanning electron microscopy (SEM) images (Figure 10) reveal that neither washing, sintering, nor combining both has a noticeable impact on the particle size or surface morphology of the NCM111 active material.

* The author's original publication.

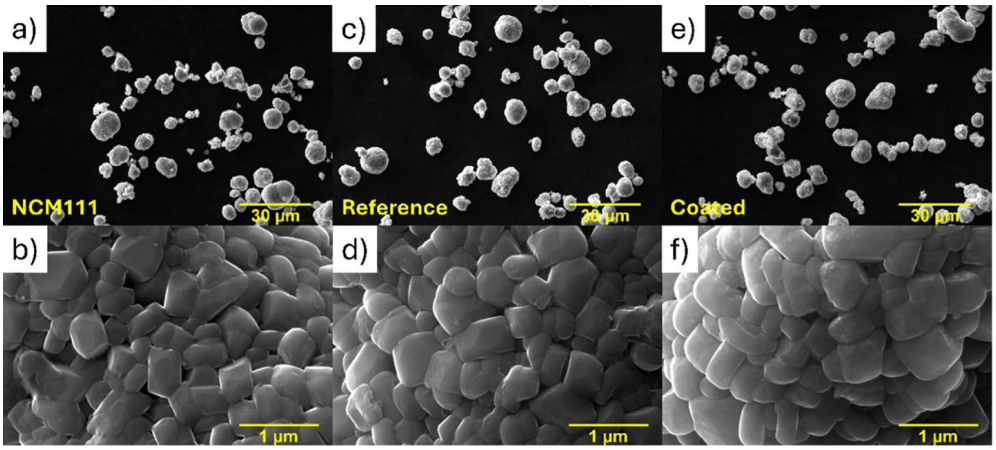

Figure 10. SEM images of pristine (a, b), reference (c, d), and coated (e, f) NCM111 material [16]*.

The presence of a nanometer-scale coating is confirmed through scanning transmission electron microscopy coupled with energy-dispersive X-ray spectroscopy (STEM-EDS) analysis (Figure 11). In the STEM bright field image (Figure 11a), the edge of a secondary particle is shown with a visible Al-containing coating approximately 10 nm thick. The red line in Figure 11a indicates the path along which the EDS line spectrum was collected spanning about 27 nm, with drift correction and approximately one spectrum captured per nanometer. As illustrated in the EDS line profile (Figure 11b), a clear decrease in Ni, Mn, and Co X-ray counts coincides with a rise in Al counts, demonstrating that the coating is localized on the particle's surface. The increase in Al signal within the 10–20 nm range of the profile further confirms the coating thickness. Additionally, Figure 11c presents the integrated line profile spectrum, where Al is distinctly visible, along with strong Ga and Pt signals originating from the protective layer deposited for analysis.

* The author's original publication.

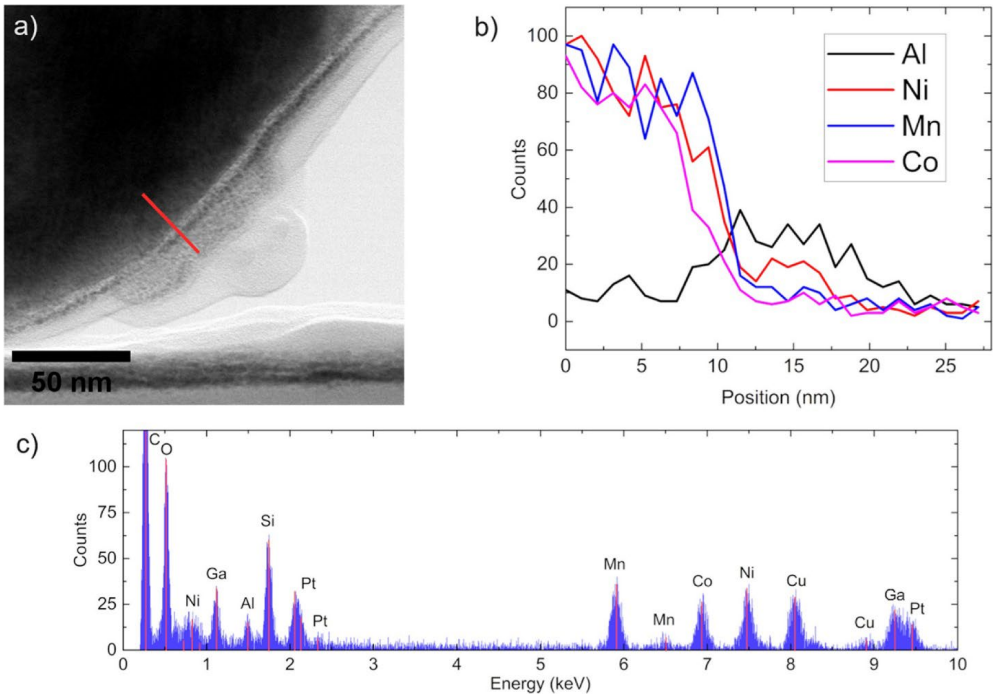

Figure 11. TEM image showing the coated NCM111 sample (a); EDS line spectrum excerpt corresponding to the red line marked in image a (b); and cumulative EDS spectrum obtained along the red line in image a (c) [16]*.

X-ray photoelectron spectroscopy (XPS) analysis of the pristine, reference, washed, sintered, and coated samples (Figure 12) highlights the changes in surface chemistry as the sample is modified. In the XPS overview all samples exhibit the characteristic peaks of Ni, Co, and Mn associated with the NCM cathode material, as seen in Figure 12a. Notably, only the coated sample displays a distinct band near 73.2 eV, corresponding to Al_2O_3 or $LiAlO_2$ [39] (Figure 12d), a feature absent in the reference and other samples. The intensity of the Al 2p peak diminishes with progressive etching, indicating that aluminum is predominantly concentrated on the surface, again confirming little to no Al diffusion into the bulk of the material. A surface-localized coating with the composition $LiAlO_2$ is consistent with expected chemical transformations during the sintering stage, where lithium from the NCM material can diffuse into the Al_2O_3 layer at elevated temperatures, forming $LiAlO_2$ [40], [41].

* The author's original publication.

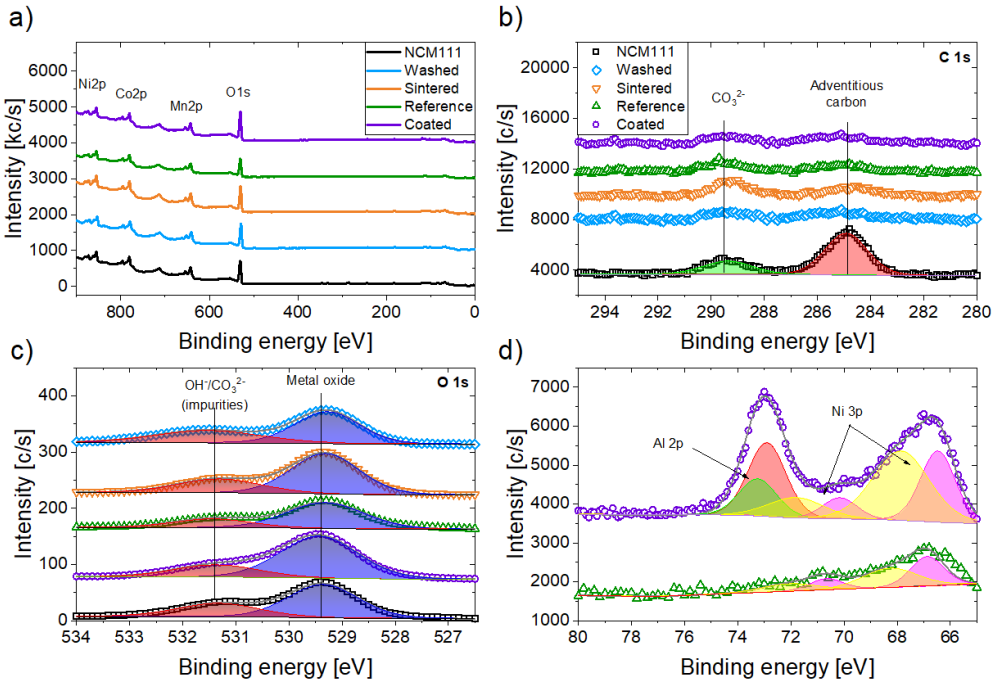

Figure 12. XPS characterisation of the synthesized materials. Survey spectra (a), C 1s spectra (b), and O 1s spectra (c) for pristine, reference, washed, sintered, and coated NCM111 samples. Al 2p spectra (d) is depicted for only reference and coated materials and shows that the coated NCM111 displays a clearly distinguishable Al 2p peak [16]*.

In the oxygen binding energy region of the XPS spectra (Figure 12c), two distinct peaks are observed at approximately 529.5 eV and 531.5 eV across all samples. These peaks correspond to lattice oxygen within the metal oxide framework of the NCM material and to surface impurities such as hydroxide (OH^-) and carbonate (CO_3^{2-}), respectively [42], [43]. In the coated sample, the metal oxide peak also includes contributions from the Al_2O_3 coating, making it slightly more prominent compared to the pristine and reference samples.

The carbon XPS spectra (Figure 12b) exhibit two distinct peaks: one at 284.8 eV corresponding to adventitious carbon (hydrocarbons adsorbed from air exposure) and another at 289.4 eV associated with surface carbonates. Among all the samples, the pristine NCM111 shows the highest intensity for the adventitious carbon peak, indicating a greater presence of surface-adsorbed hydrocarbons. Upon modification through washing, sintering, or both, this adventitious carbon signal significantly decreases, while the carbonate peak becomes more pronounced in comparison.

* The author's original publication.

Notably, the coated sample displays the weakest carbonate signal, likely due to surface coverage by $Al_2O_3/LiAlO_2$, which limits exposure. Conversely, the washed sample shows the most intense carbonate peak, even exceeding that of the adventitious carbon. This may be attributed to the ethanol washing step conducted in ambient air – since ethanol is hygroscopic, it could absorb moisture and atmospheric CO_2, promoting carbonate formation on the material's surface. Whereas the sintering step in all other modified samples removes the carbonates from the surface by burning them off. Overall, a marked reduction in carbon content is observed in the sintered, reference, and coated samples, leading to fewer side-reactions driven by RLCs.

The isotope ratio mass spectrometry (IRMS) results (Figure 13), used to quantify the carbon content in each sample, are consistent with the trends observed in the XPS data. According to IRMS measurements, the pristine and washed samples contain the highest levels of carbon. In contrast, sintering leads to a substantial reduction in carbon content, cutting it by roughly half. Three parallel IRMS analysis measurements were conducted on each sample. The error bars shown in Figure 13 reflect the standard deviation across these three measurements.

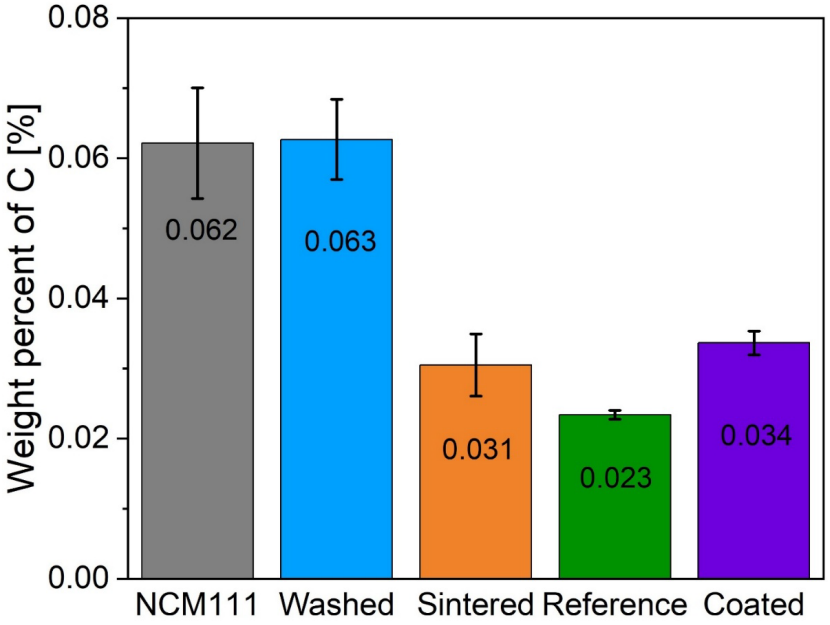

Figure 13. Carbon content analysis of all samples determined by isotope ratio mass spectrometry [16]*.

To precisely determine the aluminum concentration in the samples, inductively coupled plasma mass spectrometry (ICP-MS) analysis was conducted (Figure 14). Results indicate an Al content

* The author's original publication.

of 0.2 wt.% or 0.8 mol.%, suggesting that roughly 10 % of the aluminum introduced via AIP is successfully converted into Al_2O_3 or $LiAlO_2$ during synthesis. Additionally, a minor deficiency in Mn was consistently observed across all NCM samples. Based on the measured quantities of Li, Ni, Co, and Mn, the resulting stoichiometry is calculated as $Li_{1.07}(Ni_{0.36}Co_{0.35}Mn_{0.29})_{0.93}O_2$.

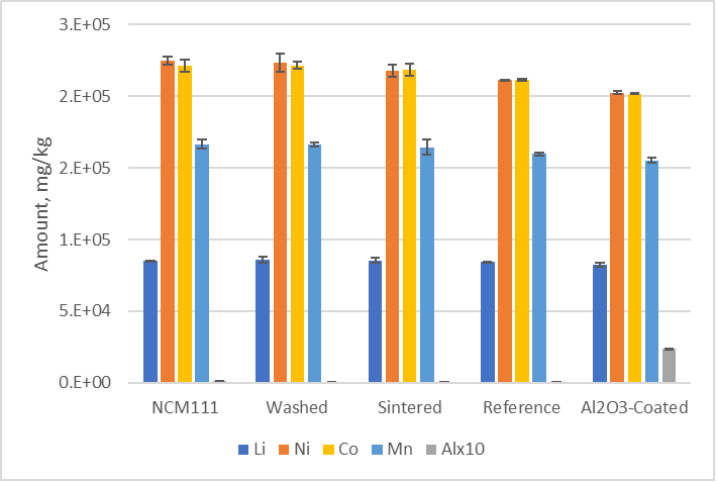

Figure 14. Amount of Li, Ni, Co, Mn and Al in all samples as determined by ICP-MS analysis [16]*.

Electrochemical Characterisation

The charge–discharge voltage profiles of all samples at 0.1 C appear similar (Figure 15b), yet the rate performance data (Figure 15a) reveal subtle but meaningful variations in lithium-ion kinetics. Among the modifications, washing NCM111 results in a noticeable reduction in discharge capacity across the full C rate range, with the most significant losses at higher rates (5 C, 10 C, and 20 C), indicating impaired electrode kinetics compared to the pristine sample. In contrast, sintering alone shows a minimal impact on rate capability at any C rate. Interestingly, when washing and sintering are combined (as in the reference sample), a slight synergistic improvement in capacity is observed at lower C rates (Figure 15a–b), although the overall rate capability remains inferior to that of the unmodified NCM111. The reduced lithium transport kinetics seen in the washed sample are also evident in the reference material. Considering the inherent variability associated with coin cell testing [35], the discharge capacities of the pristine, sintered, and coated samples may lie within experimental error margins across the entire C rate spectrum. Notably, several other studies [44]–[46] have reported enhanced or preserved rate performance when applying $LiAlO_2/Al_2O_3$ coatings, despite Al_2O_3 being an electrical insulator. These improvements in kinetics have been largely attributed to reductions in internal resistance as observed in impedance spectroscopy.

* The author's original publication.

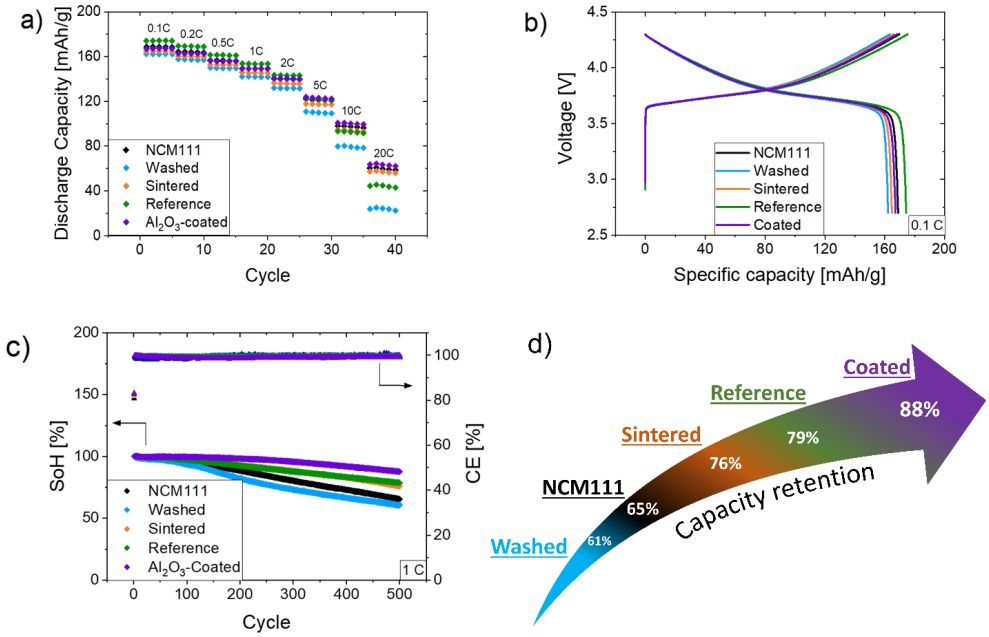

Figure 15. Rate capability measurement (a), charge–discharge curves (b), cycling stability curves (c), and illustration of the capacity retention (d) of washed, pristine, sintered, reference, and coated material [16]*.

The normalized capacity fade curve (Figure 15c) reveals that pristine NCM111 retains only 80 % of its initial capacity within the first 300 cycles, and this drops further to approximately 65 % after 500 cycles. When the NCM111 powder was washed with anhydrous ethanol and subsequently dried under vacuum at 80 °C overnight, a notable decline in performance was observed – capacity retention dropped to approximately 61 % after 500 cycles. In contrast, sintering the NCM111 powder at 500 °C in air for four hours considerably improved capacity retention, with the sample maintaining about 76 % of its initial capacity after 500 cycles. These findings align with prior studies, which report that ethanol washing removes negligible lithium [47], while sintering can reincorporate surface lithium back into the structure [3]. When both treatments (washing and sintering) were combined in the reference sample, capacity retention increased slightly to 79 % after 500 cycles. The capacity fade trend of the reference sample closely mirrored that of the sintered-only sample, implying that sintering was the dominant factor improving performance.

* The author's original publication.

Finally, the coated material demonstrates a significant improvement in cycling stability, achieving 88 % state of health (SoH) after 500 full charge-discharge cycles, indicating that the protective coating offers additional benefits that cannot be replicated by washing and sintering alone. This may be due to the coating trapping carbon impurities on the particle surface during sintering, preventing their removal. However, since these impurities are encapsulated beneath the coating, they are not directly exposed to the electrolyte and thus do not contribute to electrolyte degradation. Moreover, the $Al_2O_3/LiAlO_2$ coating can function as a scavenger for hydrofluoric acid (HF), adding another layer of protection and contributing to enhanced long-term electrochemical performance.

This research demonstrates that sintering alone can raise the SoH from 65 % to 79 % after 500 cycles, highlighting the importance of a proper reference. The coating formation, however, delivers the most substantial benefit, with the $Al_2O_3/LiAlO_2$-coated samples achieving the highest capacity retention, emphasising the importance of protective coatings in enhancing battery performance.

Summary: Wet-Chemical Coating on NCM111 Material

This research has presented a sustainable and non-toxic wet-chemical approach for applying an Al_2O_3-based coating to NCM111 cathode material for cycle life extension. Specifically, $Al_2O_3/LiAlO_2$-coated NCM111 exhibits a significant increase in cycle life, retaining 88 % of its initial capacity after 500 charge–discharge cycles, surpassing both the reference sample (79 % retention) and the untreated pristine material (66 % retention), highlighting the efficacy of the coating (Figure 15d).

A detailed investigation into each modification step has been carried out to understand their individual and combined effects on electrochemical behaviour. The analysis has revealed that washing NCM111 with anhydrous ethanol leads to performance degradation, primarily due to the formation of additional carbonate impurities on the surface. However, subsequent sintering effectively counteracts these negative effects, restoring and even improving the capacity retention relative to the pristine sample. This emphasises the critical importance of selecting a proper reference sample when assessing the benefits of surface coatings.

Taken together, the findings of this research offer a promising pathway for extending the cycle life of NCM cathode materials. The wet-chemical coating technique introduced here is especially relevant for future application in high-Ni NCM compositions, where surface instability is more pronounced. Combined with strategies such as elemental doping and microstructural optimisation, this approach could significantly improve the durability and commercial viability of next-generation lithium-ion batteries.

Wet-Chemical Coating on NCM811

As the proposed coating method proved to bring about improvements to the cycle life of NCM111 material, some initial coating tests were carried out on state-of-the-art NCM material ($Ni \geq 80$ % – NCM811) as well. Based on our previous findings about establishing a proper reference, NCM811 material was re-sintered. To check if the coating would increase the stability and prolong the cycle life of NCM811 material, long-term electrochemical charge–discharge

testing was carried out. As the coating method was not changed, in-depth structural, morphological, and chemical analysis was not performed. Additionally, cycling stability is the main indicator of the effectiveness of the coating.

Based on the previously performed meta-analysis, to most effectively protect NCM811 material from degradation both coating and doping strategies should be utilised. However, the present research focuses on coating synthesis for degradation mitigation.

The $Al_2O_3/LiAlO_2$ coating on NCM811 was deposited following the same wet-chemical synthesis procedure as for the NCM111 material. The cycling stability tests in Figure 16 reveal that although initial capacity remains unchanged (Figure 16a), some improvement can be achieved by coating the active material, increasing the SoH after 500 cycles from 44 % in the re-sintered material to 54 % in the coated material (Figure 16b). Although the improvement is minimal, it highlights that even though microcracking becomes a dominant degradation mechanism in NCM materials with Ni content over 80 %, surface protection is still useful. Additionally, the wet-chemical coating method developed on NCM111 proves to be effective, although to a lesser extent, on the NCM811 material ageing.

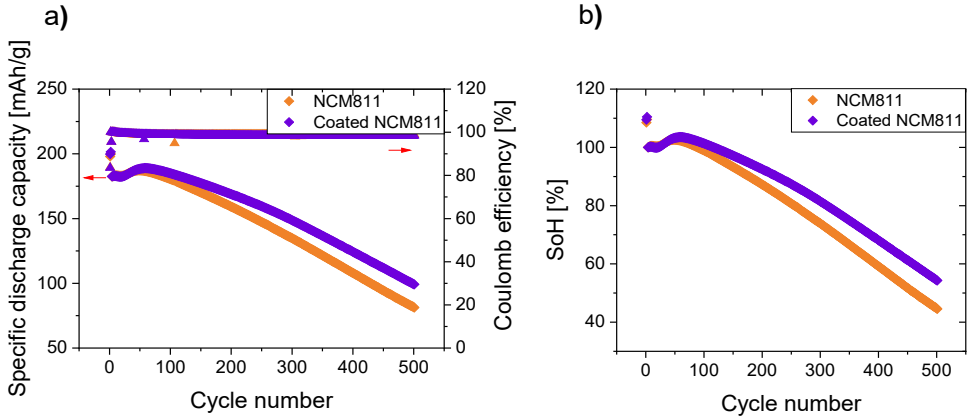

Figure 16. Cycle performance of sintered and coated NCM811 material. Discharge capacity (a) and SoH (b) as a function of cycle number.

In some cases, coating synthesis can lead to surface or even bulk doping of the coated material. It has been shown that for NCM111 Al diffusion into the bulk of the material during synthesis is hindered by Mn presence in the material. In the case of NCM811, there is considerably less Mn in the lattice, and it has been observed that Al diffusion is facilitated by the Ni-rich, Mn-poor environment [48]. Hence, some doping during sintering at high enough temperatures (800 °C) is possible in NCMs with low Mn content. In this case, sintering is performed at 500 °C, which may not be high enough to lead to Al doping. However, further in-depth XRD analysis of the lattice should be carried out to check if the lattice parameters are changed in accordance with Al doping.

Conclusions

1) Ageing in NCMs occurs both on the surface and bulk level; however, bulk degradation becomes more prominent as SoC over 80 % is reached. As for higher Ni content (≥ 80 %) NCMs 80 % SoC is reached at lower voltages (4.3 V) than for lower Ni content NCMs (~4.6 V), microcracking becomes a dominant degradation pathway for these NCMs.

2) Based on the meta-analysis, while benefits from surface protection outweigh the benefits of doping in NCM111, in NCM622 doping becomes increasingly more important in degradation mitigation, reaching an equal level of importance with surface protection in NCM811. Hence, to most effectively prevent degradation in high Ni content NCMs, both surface protection and doping strategies must be employed. This effect is consistent with the dominant ageing mechanisms, when charging to the same voltage (for example, 4.3 V).

3) The voltage hysteresis of the battery cell increases as the battery cell ages as well as with increasing specific current. The SoH of the NCM811 battery half-cell can be determined from the voltage hysteresis of the charge–discharge curve:
   a) directly from the SoH = f(ΔV) relationship, which approximates with a linear function above 70 % SoH ($R^2 = 0.9968$) and by an exponential function below 70 % SoH ($R^2 = 0.9971$).
   b) from one C rate measurement (0.1 C–2 C), fitting the obtained data points by a BV-like function (Equation (9)) and comparing the obtained curve against the graph in Figure 7c.

4) It is important to establish a proper reference in coating studies that considers the effects of the wet-chemical coating procedure (not the coating) on the material. Washing NCM with ethanol degrades performance due to carbonate impurity formation, but subsequent sintering mitigates these effects. Hence, accurate performance assessment of coatings requires careful selection of reference samples, especially when re-sintering is involved.
   a) Capacity retention of pristine (as-obtained) NCM111 material after 500 cycles at 1 C rate is 65 % whereas the material that underwent the coating procedure (without Al precursor) shows a capacity retention of 79 %.
   b) After washing the sample in ethanol (the first part of the coating procedure) capacity retention decreases to 61 %, whereas after only sintering the material at 500 °C in air the capacity retention increases to 76 % after 500 cycles at 1 C rate. This indicates that of the two steps involved in the coating procedure, sintering provides the most significant improvement in cycle life.

5) The developed wet-chemically produced $Al_2O_3/LiAlO_2$ coating provides improvements in the cycle life of NCM111 material. Capacity retention after 500 cycles at 1 C rate for the coated sample is 88 %, which is a notable improvement in the capacity retention of both the pristine (65 %) and reference (79 %) samples.

6) The same wet-chemical coating method can be used to improve the cycle life of NCM811 material. The capacity retention after 500 cycles at 1 C rate improved from 44 % in the re-sintered (reference) material to 54 % in the coated material.

7) Based on the conducted meta-analysis, in addition to the applied coating, further improvements to capacity retention in NCM811 material could be achieved by elemental doping.

References

[1] M. Jiang, D. L. Danilov, R.-A. Eichel, and P. H. L. Notten, 'A Review of Degradation Mechanisms and Recent Achievements for Ni-Rich Cathode-Based Li-Ion Batteries', *Adv. Energy Mater.*, vol. 11, no. 48, p. 2103005, 2021, doi: 10.1002/aenm.202103005.

[2] W. Li, H. Y. Asl, Q. Xie, and A. Manthiram, 'Collapse of $LiNi_{1-x-y}Co_xMn_yO_2$ Lattice at Deep Charge Irrespective of Nickel Content in Lithium-Ion Batteries', *J. Am. Chem. Soc.*, vol. 141, no. 13, pp. 5097–5101, Apr. 2019, doi: 10.1021/jacs.8b13798.

[3] B. Huang, D. Liu, K. Qian, L. Zhang, K. Zhou, Y. Liu, F. Kang, B. Li, 'A Simple Method for the Complete Performance Recovery of Degraded Ni-rich $LiNi_{0.70}Co_{0.15}Mn_{0.15}O_2$ Cathode via Surface Reconstruction', *ACS Appl. Mater. Interfaces*, vol. 11, no. 15, pp. 14076–14084, Apr. 2019, doi: 10.1021/acsami.8b22529.

[4] J. Li, S. Wang, L. Chen, Y. Wang, H. Zhou, and J. M. Guerrero, 'Adaptive Kalman filter and self-designed early stopping strategy optimized convolutional neural network for state of energy estimation of lithium-ion battery in complex temperature environment', *J. Energy Storage*, vol. 83, p. 110750, Apr. 2024, doi: 10.1016/j.est.2024.110750.

[5] L. Vichard, A. Ravey, P. Venet, F. Harel, S. Pelissier, and D. Hissel, 'A method to estimate battery SOH indicators based on vehicle operating data only', *Energy*, vol. 225, p. 120235, Jun. 2021, doi: 10.1016/j.energy.2021.120235.

[6] S. Wang, Y. Fan, S. Jin, P. Takyi-Aninakwa, and C. Fernandez, 'Improved anti-noise adaptive long short-term memory neural network modeling for the robust remaining useful life prediction of lithium-ion batteries', *Reliab. Eng. Syst. Saf.*, vol. 230, p. 108920, Feb. 2023, doi: 10.1016/j.ress.2022.108920.

[7] B. Lu, Y. Song, Q. Zhang, J. Pan, Y.-T. Cheng, and J. Zhang, 'Voltage hysteresis of lithium ion batteries caused by mechanical stress', *Phys. Chem. Chem. Phys.*, vol. 18, no. 6, pp. 4721–4727, Feb. 2016, doi: 10.1039/C5CP06179B.

[8] V. J. Ovejas and A. Cuadras, 'Effects of cycling on lithium-ion battery hysteresis and overvoltage', *Sci. Rep.*, vol. 9, no. 1, p. 14875, Oct. 2019, doi: 10.1038/s41598-019-51474-5.

[9] V. J. Ovejas and A. Cuadras, 'State of charge dependency of the overvoltage generated in commercial Li-ion cells', *J. Power Sources*, vol. 418, pp. 176–185, Apr. 2019, doi: 10.1016/j.jpowsour.2019.02.046.

[10] J. Newman and N. P. Balsara, *Electrochemical Systems*, 4th ed. John Wiley & Sons, 2021.

[11] S. Ernst, T. P. Heins, N. Schlüter, and U. Schröder, 'Capturing the Current-Overpotential Nonlinearity of Lithium-Ion Batteries by Nonlinear Electrochemical Impedance Spectroscopy (NLEIS) in Charge and Discharge Direction', *Front. Energy Res.*, vol. 7, Dec. 2019, doi: 10.3389/fenrg.2019.00151.

[12] 'Butler–Volmer equation', *Wikipedia*. Jul. 20, 2024. Accessed: Feb. 02, 2025. [Online]. Available: https://en.wikipedia.org/w/index.php?title=Butler%E2%80%93Volmer_equation&oldid=1235622157

[13] L. Britala, M. Marinaro, and G. Kucinskis, 'A review of the degradation mechanisms of NCM cathodes and corresponding mitigation strategies', *J. Energy Storage*, vol. 73, p. 108875, Dec. 2023, doi: 10.1016/j.est.2023.108875.

[14] Y. Jiang, Y. Bi, M. Liu, Z. Peng, L. Huai, P. Don, J. Duan, Z. Chen, X. Li, D. Wang, and Y. Zhang, 'Improved stability of Ni-rich cathode by the substitutive cations with stronger

bonds', *Electrochimica Acta*, vol. 268, pp. 41–48, Apr. 2018, doi: 10.1016/j.electacta.2018.01.119.

[15] M. Dixit, B. Markovsky, D. Aurbach, and D. T. Major, 'Unraveling the Effects of Al Doping on the Electrochemical Properties of $LiNi_{0.5}Co_{0.2}Mn_{0.3}O_2$ Using First Principles', *J. Electrochem. Soc.*, vol. 164, no. 1, p. A6359, Jan. 2017, doi: 10.1149/2.0561701jes.

[16] L. Maskova, R. Ignatans, A. Viksna, A. Sarakovskis, M. Knite, and G. Kucinskis, 'Wet-Chemical Synthesis of a Protective Coating on NCM111 Cathode: The Quantified Effects of Washing, Sintering and Coating', *J. Electrochem. Soc.*, vol. 171, no. 10, p. 100520, Oct. 2024, doi: 10.1149/1945-7111/ad8483.

[17] H. Zhang, J. Xu, and J. Zhang, 'Surface-Coated $LiNi_{0.8}Co_{0.1}Mn_{0.1}O_2$ (NCM811) Cathode Materials by Al_2O_3, ZrO_2, and Li_2O-$2B_2O_3$ Thin-Layers for Improving the Performance of Lithium Ion Batteries', *Front. Mater.*, vol. 6, Nov. 2019, doi: 10.3389/fmats.2019.00309.

[18] G. Kaur and B. D. Gates, 'Review—Surface Coatings for Cathodes in Lithium Ion Batteries: From Crystal Structures to Electrochemical Performance', *J. Electrochem. Soc.*, vol. 169, no. 4, p. 043504, Apr. 2022, doi: 10.1149/1945-7111/ac60f3.

[19] B. Han, T. Pulauskas, B. Key, C. Peebles, J. S. Park, R. F. Klie, J. T. Vaughey, and F. Dogan, 'Understanding the Role of Temperature and Cathode Composition on Interface and Bulk: Optimizing Aluminum Oxide Coatings for Li-Ion Cathodes', *ACS Appl. Mater. Interfaces*, vol. 9, no. 17, pp. 14769–14778, May 2017, doi: 10.1021/acsami.7b00595.

[20] D. Hu, F. Du, H. Cao, Q. Zhou, P. Sun, T. Xu, C. Mei, Q. Hao, Z. Fan, and J. Zheng, 'An effective strategy to control thickness of Al_2O_3 coating layer on nickel-rich cathode materials', *J. Electroanal. Chem.*, vol. 880, p. 114910, Jan. 2021, doi: 10.1016/j.jelechem.2020.114910.

[21] X. Xiong, Z. Wang, P. Yue, H. Guo, F. Wu, J. Wang, and X. Li, 'Washing effects on electrochemical performance and storage characteristics of $LiNi_{0.8}Co_{0.1}Mn_{0.1}O_2$ as cathode material for lithium-ion batteries', *J. Power Sources*, vol. 222, pp. 318–325, Jan. 2013, doi: 10.1016/j.jpowsour.2012.08.029.

[22] Y. Su, G. Chen, L. Chen, L. Li, C. Li, R. Ding, J. Liu, Z. Lu, Y. Lu, L. Bao, G. Tan, S. Chen, and F. Wu, 'Clean the Ni-Rich Cathode Material Surface With Boric Acid to Improve Its Storage Performance', *Front. Chem.*, vol. 8, Jul. 2020, doi: 10.3389/fchem.2020.00573.

[23] S. J. Shi, J. P. Tu, Y. J. Mai, Y. Q. Zhang, Y. Y. Tang, and X. L. Wang, 'Structure and electrochemical performance of CaF_2 coated $LiMn_{1/3}Ni_{1/3}Co_{1/3}O_2$ cathode material for Li-ion batteries', *Electrochimica Acta*, vol. 83, pp. 105–112, Nov. 2012, doi: 10.1016/j.electacta.2012.08.029.

[24] H. K. Kim, H. S. Kang, P. Santhoshkumar, J. W. Park, C. W. Ho, G. S. Sim, and C. W. Lee, 'Surface modification of Ni-rich $LiNi_{0.8}Co_{0.1}Mn_{0.1}O_2$ with perovskite $LaFeO_3$ for high voltage cathode materials', *RSC Adv.*, vol. 11, no. 35, pp. 21685–21694, Jun. 2021, doi: 10.1039/D1RA00857A.

[25] S. She, Y. Zhou, Z. Hong, Y. Huang, and Y. Wu, 'Surface Coating of NCM-811 Cathode Materials with g-C_3N_4 for Enhanced Electrochemical Performance', *ACS Omega*, vol. 7, no. 28, pp. 24851–24857, Jul. 2022, doi: 10.1021/acsomega.2c03074.

[26] W. Cho, S.-M. Kim, K.-W. Lee, J. H. Song, Y. N. Jo, T. Yim, H. Kim, J.-S. Kim, and Y.-J. Kim, 'Investigation of new manganese orthophosphate $Mn_3(PO_4)_2$ coating for nickel-rich $LiNi_{0.6}Co_{0.2}Mn_{0.2}O_2$ cathode and improvement of its thermal properties', *Electrochimica Acta*, vol. 198, pp. 77–83, Apr. 2016, doi: 10.1016/j.electacta.2016.03.079.

[27] R. Jung, M. Metzger, F. Maglia, C. Stinner, and H. A. Gasteiger, 'Oxygen Release and Its Effect on the Cycling Stability of $LiNi_xMn_yCo_zO_2$ (NMC) Cathode Materials for Li-Ion

Batteries', *J. Electrochem. Soc.*, vol. 164, no. 7, p. A1361, May 2017, doi: 10.1149/2.0021707jes.

[28] W. Xiao, Y. Nie, C. Miao, J. Wang, Y. Tan, and M. Wen, 'Structural design of high-performance Ni-rich $LiNi_{0.83}Co_{0.11}Mn_{0.06}O_2$ cathode materials enhanced by Mg^{2+} doping and Li_3PO_4 coating for lithium ion battery', *J. Colloid Interface Sci.*, vol. 607, pp. 1071–1082, Feb. 2022, doi: 10.1016/j.jcis.2021.09.067.

[29] J. Hodakovska, L. Britala, A. Mezulis, L. Grinberga, G. Bajars, and G. Kucinskis, 'State of health as a function of voltage hysteresis in Li-ion battery half-cells', *J. Solid State Electrochem.*, Jun. 2024, doi: 10.1007/s10008-024-05944-0.

[30] J. Seok, C. N. Gannett, S.-H. Yu, and H. D. Abruña, 'Understanding the Impacts of Li Stripping Overpotentials at the Counter Electrode by Three-Electrode Coin Cell Measurements', *Anal. Chem.*, vol. 93, no. 46, pp. 15459–15467, Nov. 2021, doi: 10.1021/acs.analchem.1c03422.

[31] W. Dreyer, J. Jamnik, C. Guhlke, R. Huth, J. Moškon, and M. Gaberšček, 'The thermodynamic origin of hysteresis in insertion batteries', *Nat. Mater.*, vol. 9, no. 5, Art. no. 5, May 2010, doi: 10.1038/nmat2730.

[32] T. Katrašnik, J. Moškon, K. Zelič, I. Mele, F. Ruiz-Zepeda, and M. Gaberšček, 'Entering Voltage Hysteresis in Phase-Separating Materials: Revealing the Electrochemical Signature of the Intraparticle Phase-Separated State', *Adv. Mater.*, vol. 35, no. 31, p. 2210937, 2023, doi: 10.1002/adma.202210937.

[33] J. Lim, Y. Li, D. H. Alsem, H. So, S. C. Lee, P. Bai, D. A. Cogswell, X. Liu, N. Jin, Y.-S. Yu, N. J. Salmon, D. A. Shapiro, M. Z. Bazant, T. Tyliszczak, and W. C. Chueh, 'Origin and hysteresis of lithium compositional spatiodynamics within battery primary particles', *Science*, vol. 353, no. 6299, pp. 566–571, Aug. 2016, doi: 10.1126/science.aaf4914.

[34] Y. Li, S. Meyer, J. Lim, S. C. Lee, W. E. Gent, S. Marchesini, H. Krishnan, T. Tyliszczak, D. Shapiro, A. L. D. Kilcoyne, and W. C. Chueh, 'Effects of Particle Size, Electronic Connectivity, and Incoherent Nanoscale Domains on the Sequence of Lithiation in $LiFePO_4$ Porous Electrodes', *Adv. Mater.*, vol. 27, no. 42, pp. 6591–6597, 2015, doi: 10.1002/adma.201502276.

[35] A. Smith, P. Stüble, L. Leuthner, A. Hofmann, F. Jeschull, and L. Mereacre, 'Potential and Limitations of Research Battery Cell Types for Electrochemical Data Acquisition', *Batter. Supercaps*, vol. 6, no. 6, p. e202300080, 2023, doi: 10.1002/batt.202300080.

[36] A. Ponrouch and M. R. Palacín, 'On the impact of the slurry mixing procedure in the electrochemical performance of composite electrodes for Li-ion batteries: A case study for mesocarbon microbeads (MCMB) graphite and Co_3O_4', *J. Power Sources*, vol. 196, no. 22, pp. 9682–9688, Nov. 2011, doi: 10.1016/j.jpowsour.2011.07.045.

[37] A. O. Kondrakov, A. Schmidt, J. Xu, H. Geßwein, R. Mönig, P. Hartmann, H. Sommer, T. Brezesinski, and J. Janek, 'Anisotropic Lattice Strain and Mechanical Degradation of High- and Low-Nickel NCM Cathode Materials for Li-Ion Batteries', *J. Phys. Chem. C*, vol. 121, no. 6, pp. 3286–3294, Feb. 2017, doi: 10.1021/acs.jpcc.6b12885.

[38] W. Hua, B. Schwarz, M. Knapp, A. Senyshyn, A. Missiul, X. Mu, S. Wang, C. Kübel, J. R. Binder, S. Indris, and H. Ehrenberg, '(De)Lithiation Mechanism of Hierarchically Layered $LiNi_{1/3}Co_{1/3}Mn_{1/3}O_2$ Cathodes during High-Voltage Cycling', *J. Electrochem. Soc.*, vol. 166, no. 3, p. A5025, Nov. 2018, doi: 10.1149/2.0051903jes.

[39] R. S. Negi, Y. Yusim, R. Pan, S. Ahmed, K. Volz, R. Takata, F. Schmidt, A. Henss, and M. T. Elm, 'A Dry-Processed $Al_2O_3/LiAlO_2$ Coating for Stabilizing the

Cathode/Electrolyte Interface in High-Ni NCM-Based All-Solid-State Batteries', *Adv. Mater. Interfaces*, vol. 9, no. 8, p. 2101428, 2022, doi: 10.1002/admi.202101428.

[40] O. Touag, G. Coquil, M Charbonneau, G. Foran, A. Ghosh, D. Mankovsky, and M. Dollé, 'One-pot synthesis of $LiAlO_2$-coated $LiNi_{0.6}Mn_{0.2}Co_{0.2}O_2$ cathode material', *Energy Adv.*, vol. 2, no. 5, pp. 701–711, May 2023, doi: 10.1039/D3YA00061C.

[41] J. L. White, F. S. Gittleson, M. Homer, and F. El Gabaly, 'Nickel and Cobalt Oxidation State Evolution at Ni-Rich NMC Cathode Surfaces during Treatment', *J. Phys. Chem. C*, vol. 124, no. 30, pp. 16508–16514, Jul. 2020, doi: 10.1021/acs.jpcc.0c04794.

[42] R. Li, Y. Ming, W. Xiang, C. Xu, G. Feng, Y. Li, Y. Chen, Z. Wu, B. Zhong, and X. Guo, 'Structure and electrochemical performance modulation of a $LiNi_{0.8}Co_{0.1}Mn_{0.1}O_2$ cathode material by anion and cation co-doping for lithium ion batteries', *RSC Adv.*, vol. 9, no. 63, pp. 36849–36857, Nov. 2019, doi: 10.1039/C9RA07873H.

[43] X. Ren, J. Du, Z. Pu, R. Wang, L. Gan, and Z. Wu, 'Facile synthesis of Li_2MoO_4 coated $LiNi_{1/3}Co_{1/3}Mn_{1/3}O_2$ composite as a novel cathode for high-temperature lithium batteries', *Ionics*, vol. 26, no. 4, pp. 1617–1627, Apr. 2020, doi: 10.1007/s11581-020-03474-z.

[44] R. S. Negi, S. P. Culver, A. Mazilkin, T. Brezesinski, and M. T. Elm, 'Enhancing the Electrochemical Performance of $LiNi_{0.70}Co_{0.15}Mn_{0.15}O_2$ Cathodes Using a Practical Solution-Based Al_2O_3 Coating', *ACS Appl. Mater. Interfaces*, vol. 12, no. 28, pp. 31392–31400, Jul. 2020, doi: 10.1021/acsami.0c06484.

[45] A. Zhou, Q. Liu, Y. Wang, W. Wang, X. Yao, W. Hu, L. Zhang, X. Yu, J. Li, and H. Li, 'Al_2O_3 surface coating on $LiCoO_2$ through a facile and scalable wet-chemical method towards high-energy cathode materials withstanding high cutoff voltages', *J. Mater. Chem. A*, vol. 5, no. 46, pp. 24361–24370, Nov. 2017, doi: 10.1039/C7TA07312G.

[46] J. Cho, Y. J. Kim, and B. Park, 'Novel $LiCoO_2$ Cathode Material with Al_2O_3 Coating for a Li Ion Cell', *Chem. Mater.*, vol. 12, no. 12, pp. 3788–3791, Dec. 2000, doi: 10.1021/cm000511k.

[47] Y. Zhou, Z. Hu, Y. Huang, Y. Wu, and Z. Hong, 'Effect of solution wash on the electrochemical performance of $LiNi_{0.8}Co_{0.1}Mn_{0.1}O_2$ cathode materials', *J. Alloys Compd.*, vol. 888, p. 161584, Dec. 2021, doi: 10.1016/j.jallcom.2021.161584.

[48] B. Han, B. Key, S. H. Lapidus, J. C. Garcia, H. Iddir, J. T. Vaughey, and F. Dogan, 'From Coating to Dopant: How the Transition Metal Composition Affects Alumina Coatings on Ni-Rich Cathodes', *ACS Appl. Mater. Interfaces*, vol. 9, no. 47, pp. 41291–41302, Nov. 2017, doi: 10.1021/acsami.7b13597.

Līga Maskova was born in 1995 in Riga. She obtained a Bachelor's degree in Chemistry from the University of Latvia (UL) (2019) and a Master's degree with distinction in Materials Science and Technology from the University of Tartu (2021). She has worked at the Institute of Organic Synthesis, the Institute of Chemical Physics, and the Thin-Film Technology Laboratory at the University of Tartu, holding Laboratory Technician/Specialist positions. She is currently a Researcher at the UL Institute of Solid State Physics. Her research interests include enhancing renewable energy storage capacity in next-generation lithium-ion and sodium-ion batteries, as well as reducing battery waste through effective identification and mitigation of ageing processes